EXPERIMENTATION OF MODE I & MODE II FRACTURE OF UNI-DIRECTIONAL COMPOSITES AND FINITE ELEMENT ANALYSIS OF MODE I FRACTURE USING COHESIVE CONTACT

A Thesis

presented to

the Faculty of California Polytechnic State University,

San Luis Obispo

In Partial Fulfillment

of the Requirements for the Degree

Master of Science in Mechanical Engineering

by

Joseph D. Garrett

September 2016

COMMITTEE MEMBERSHIP

TITLE:	Experimentation of Mode I & Mode II Fracture of Uni-Directional Composites and Finite Element Analysis of Mode I Fracture Using Cohesive Contact
AUTHOR:	Joseph D. Garrett
DATE SUBMITTED:	September 2016
COMMITTEE CHAIR:	Joseph Mello, Ph.D. Professor of Mechanical Engineering
COMMITTEE MEMBER:	John Chen, Ph.D. Professor of Mechanical Engineering
COMMITTEE MEMBER:	Thomas Mase, Ph.D. Professor of Mechanical Engineering

ABSTRACT

Experimentation of Mode I & Mode II Fracture of Uni-Directional Composites and Finite Element Analysis of Mode I Fracture Using Cohesive Contact

Joseph D. Garrett

As the use of fiber-reinforced composites has increased over the decades, so has the need to understand the complexity of their failure mechanisms as engineers seek to improve the damage tolerance of composite laminated structures. One of the most prevalent and limiting mode of failure within composite laminates is delamination, since it not only reduces a structures stiffness and strength, but can be very difficult to detect without the use of special non-destructive equipment. Industry testing organizations have utilized several fracture tests in order to characterize the fracture toughness of composite materials under different loading conditions. For this research, ASTM D5528, ASTM D7905 & 4ENF tests were performed to evaluate the fracture resistance of uni-directional pre-preg laminates; the 4ENF was used to compare its effectiveness to ASTM D7905.

Finite element methods such as the use of cohesive elements have been developed to simulate delamination within composite laminates. While there has been much work in evaluating the effectiveness of cohesive elements, very little exists within literature as to studying the success of cohesive surface contact for accurately modeling coupon level fracture testing. Cohesive contact interaction in Abaqus/Standard was used to simulate the mode I double cantilever beam (DCB) experiment of ASTM D5528. Cohesive contact was found to accurately and efficiently model DCB testing as the critical load-displacement values and steady state fracture agreed with experimental data. A parametric study was performed and found that cohesive contact was less sensitive in varying key model parameters than that commonly expected of cohesive elements.

ACKNOWLEDGMENTS

I want to thank my family for all of their support over the years while attending Cal Poly, especially during my graduate studies. I thank my mom for all the times in which I know she was praying for me to get through school; and to speak on the phone when I was stressed, her support is unmatched except for God Himself.

I would like to thank my thesis committee for all of the help and great advice that was given to me during my research. Dr. Mase provided me with insight into finite element modeling and challenged me theoretically in understanding material failure. Dr. Chen taught me how to make delaminated composite specimens and made time for me whenever I had questions or needed help with testing. As for Dr. Mello, I am sometimes surprised that he has put up with me over the three years of knowing him. In that time, I have worked for him on several occasions as a grader/student assistant and was lucky to have him for what ended up as two of my favorite courses at Cal Poly: finite element analysis and composites. I was incredibly fortunate to work with him as a teaching assistant for his composites course: I saw firsthand the challenges in teaching college students, but also the joy that came from influencing their lives by sharing knowledge. It has been a privilege to work with Dr. Mello and to have him as my thesis advisor, I have grown tremendously from these experiences and I would not have had them without his council and support.

I want to thank my dear friends Jeremy Depangher and Sean Kennedy for their unconditional love and support during the arduous times of my educational career. You two know how much you truly mean to me. I would like to give special thanks to my

fellow graduate students and close friends, Grant Wittenberg, Peter Rivera and George Rodriguez. Towards the last several weeks of my research, Grant sacrificed his time to help me in the composites lab with testing as well as general advice for my work. Peter and I have been in the trenches together at Poly for several years and I would not have had it any other way; his honesty and objectivity have helped me to remain focused on the goals at hand, as we have sharpened one another as friends. George and I spent way too much time in the composites lab laying up, curing, and testing our composite specimens. Thank you George for all of the hours we spent in the grad lab discussing our thesis projects and all the bantering when we had to wait for our FE simulations to converge (if they ever did!).

Lastly and of most importance to me, I want to thank my God and Savior Christ Jesus. I would not have been able to complete my degrees or finish my thesis without Him. For the first years of college I did not think that I would ever graduate, let alone from Cal Poly San Luis Obispo with a master's degree in mechanical engineering. I owe Him my life and my gratitude. Through all the trials and inconsistency of life, He has been the one constant and has sustained me in all that I have done. I give Him all praise and I hope this work will bring glory to His name. Thank you Jesus. Amen.

Romans 5:1-9

5 Therefore being justified by faith, we have peace with God through our Lord Jesus Christ:

2 By whom also we have access by faith into this grace wherein we stand, and rejoice in hope of the glory of God.

3 And not only so, but we glory in tribulations also: knowing that tribulation worketh patience;

4 And patience, experience; and experience, hope:

5 And hope maketh not ashamed; because the love of God is shed abroad in our hearts by the Holy Ghost which is given unto us.

6 For when we were yet without strength, in due time Christ died for the ungodly.

7 For scarcely for a righteous man will one die: yet peradventure for a good man some would even dare to die.

8 But God commendeth his love toward us, in that, while we were yet sinners, Christ died for us.

9 Much more then, being now justified by his blood, we shall be saved from wrath through him.

TABLE OF CONTENTS

Page

LIST OF TABLES

Table Page

LIST OF FIGURES

Figure Page

LIST OF SYMBOLS

σ_{ij}	Stress tensor
ϵ_{ij}	Strain tensor
δ_{ij}	Knocker delta
ϵ_{kk}	Trace of strain tensor
τ	Shear stress
$[\bar{Q}]$	Composite stiffness matrix
$\{N\}$	Resultant normal & shear line loads
$\{M\}$	Resultant bending & twisting line moments
A_{ij}	Laminate extensional stiffness matrix
B_{ij}	Laminate extensional/bending coupling stiffness matrix
D_{ij}	Laminate bending stiffness matrix
a	Delamination/crack length
K	Stress intensity
G	Strain energy release rate (SERR)
r_y	Process zone length
C	Compliance
D	Scalar damage variable
a_0	Initial delamination/crack length
G_{IC}	Critical mode I fracture energy
G_{IIC}	Critical mode II fracture energy
G_{IIIC}	Critical mode III fracture energy
l_{cz_I}	Mode I cohesive zone length
l_e	Element length
N_e	Number of elements within cohesive zone

CHAPTER 1: INTRODUCTION

1.1 Damage Tolerance

Damage tolerance has become an essential area of research for engineers as they seek to increase the life of materials for their respective engineering applications. Since the early/mid-20th century, much research has been put into studying damage tolerance within metals like aluminum and steel; such as creep, fatigue & fracture, and environmental effects. As the research efforts have increased over the years in characterizing engineering materials, so has the complexity and performance of newer materials such as fiber reinforced composites. With the increase in use of carbon fiber reinforced polymer's (CFRP's), especially throughout the aerospace industry, the research of damage tolerance within composite materials is still a major area of interest and study throughout academia and industry.

Composite materials though, are not as well understood and characterized as their metal counterparts. Their unique microstructure gives rise to complex modes of failure that can be difficult to characterize and predict. Such failure modes include fiber fracture, matrix cracking and interlaminar delamination. Delamination is a common failure mode that is of major concern as it is possibly the most limiting mode of failure within composites: delaminations are typically undetectable and result in a loss of strength and stiffness of the composite structure. A delamination can be viewed as a crack that occurs in-between two plies within the composite laminate. Once a delamination occurs, the structure is susceptible to delamination propagation and can result in catastrophic fracture. Delamination resistance is characterized by a mechanical property known as

“fracture toughness” or “fracture strength” and it is dominated by the matrix constituent of the composite laminate.

Fracture testing has been performed since the 1970’s to characterize the fracture toughness of composite materials; with several testing methods having been standardized by American Society for Testing & Materials (ASTM). Fracture test specimens are manufactured with a built-in delamination in order to simulate the presence of delamination(s) within composite structures. Coupon level testing leads to obtaining a materials fracture toughness which can be used as an optimization parameter in design when considering damage tolerance of a given structure. Various fracture tests are performed to capture a materials fracture response when subjugated to different modes of fracture. Numerical techniques have been developed to simulate these tests in order to minimize the amount of coupon level testing required for design optimization and damage tolerance considerations.

Finite element analysis tools such as Abaqus/Standard are used to model fracture, more specifically, the onset and propagation of delaminations within composite structures. Numerical schemes such as Virtual Crack Closure Technique (VCCT) and Cohesive Zone Modeling (CZM) are available in several FEA packages for engineers to calibrate model parameters in order to simulate composite fracture testing and overall structural response.

1.2 Thesis Goals

This thesis is a continuation and further development of the work done by Josh Smith at Cal Poly San Luis Obispo [1]. The goals of this thesis were as followes:

- Perform mode I & mode II fracture testing per standards ASTM D5528 & ASTM D7905 respectively.
- Perform alternative mode II test not standardized by ASTM, and compare to ASTM D7905.
- Test fracture specimens with both PTFE & mold release built-in delamination methods.
- Use cohesive contact interaction within Abaqus/Standard to calibrate a model of mode I testing done by Josh Smith [1] and the mode I testing laid out in this thesis.
- Perform a parametric study to investigate the sensitivity of FE model parameters within Abaqus/Standard cohesive contact modeling.

CHAPTER 2: COMPOSITE FAILURE AND FRACTURE ANALYSIS

2.1 Introduction

Due to the more complex microstructure of composite laminated structures, the methods behind analyzing them are innately more intricate as compared to metals. Commonly used engineering materials such as aluminum and steel have a homogenous microstructure and exhibit isotropic behavior: properties do not vary point to point and material behavior is independent of reference axes. Composite materials, depending their ply layup, will instead exhibit orthotropic and anisotropic behavior. A material is classified as orthotropic when there exists three mutually perpendicular, orthogonal planes of material symmetry; such as wood or cross-ply composite laminates. The intersection of these planes define “Principal Material Axes” (PMA’s) or “material bases”. Anisotropy on the other hand occurs when the material properties at a point vary with direction and are a function of the reference axes orientation. No planes of material symmetry exists within anisotropic materials; some examples include biological tissues such as tendons & ligaments. A visual demonstration of material symmetries is seen in Figure 1.

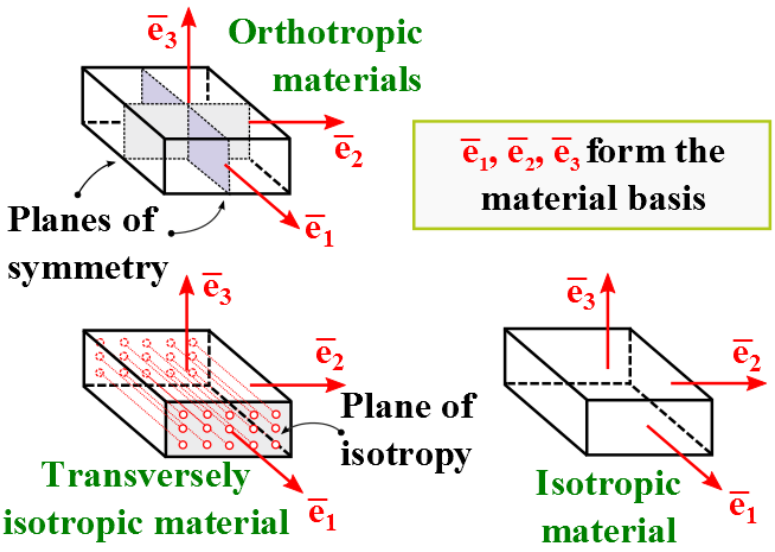

Figure 1 Material bases' for orthotropic, transversely isotropic and isotropic materials [2].

A sub class of orthotropy is transverse isotropy and is the material classification for when a single ply of composite is considered. A material is deemed to be transversely isotropic when a single plane of material symmetry exists; isotropic behavior will occur in that plane. Transverse isotropy also applies to uni-directional laminates as the fibers all run in the same direction. In special cases, laminates can have an in-plane isotropic response known as “quasi-isotropic”. This response is not entirely isotropic because the corresponding isotropy is only in the plane of the laminate; the response through the thickness is not the same as that in plane, hence 3D isotropy does not apply.

Different material classifications arise to different ways in which a structure can fail. The complexity of potential failure within a material is tied to its microstructure; consider an isotropic metal, it’s potential modes of failure are not as complex as that of a composite laminate, and are easier to predict/analyze as well. Understanding the intricacies behind composite failure is important because a laminated structure will most

likely have an orthotropic or anisotropic material classification, and can exhibit multiple failure modes simultaneously during loading. Complex failure can also occur within transversely isotropic or quasi-isotropic laminates as matrix cracking, fiber fracture and delamination are all of major concern.

2.2 Composite Failure

Ductile materials such as metals will typically fail due to plastic deformation, whereas brittle materials, like ceramics, do not show signs of yielding before failure and instead rupture catastrophically. Composite structures on the other hand have many ways in which they can fail, and are not limited to having multiple modes of failure occurring at the same time. Some of the common failure modes include; matrix cracking, fiber fracture, fiber debonding and interlaminar delamination; these can be seen below in Figure 2 Common failure modes for composite structures. Figure 2.

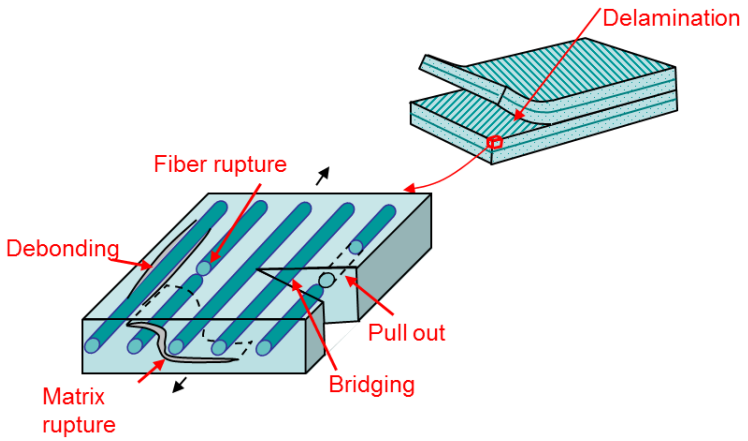

Figure 2 Common failure modes for composite structures. [3]

The occurrence of a particular failure mode can depend on the following parameters; the manner in which stored elastic strain energy is released, how flaws are distributed throughout the laminate, and on the toughness of the fiber-matrix interface, as well as the matrix itself [4]. One of the advantages of composite structures is the ability to tailor structures' strength and stiffness in a preferred direction. With this benefit though, comes the fact that the matrix constituent is weaker and is susceptible to failure if the matrix must support mechanical loading in another direction.

Matrix failure can occur through several means; excessive shear, transverse cracking along and between the fibers, as well interlaminar delamination. Once matrix cracking occurs and propagates, fibers could begin to fail by fiber fracture and will do so locally relative to the origin of matrix cracking. If the matrix is tough and ductile, or there is an inclusion within a fiber, then the most likely mode of failure will be due to fiber fracture. Fiber fracture occurs when the mechanical loads within the laminate induce stresses that exceed the strength of the fiber; since the fibers are brittle and linear elastic, they will fail without yielding and do so catastrophically. Upon a fiber failing, the load path is then changed and surrounding fibers will have to carry the mechanical load and will be more susceptible to fracture if the fiber strength is again exceeded. If the matrix has a high fracture toughness and an adequate fiber-matrix bond is present, than a relatively low amount of strain energy is released during fiber fracture as compared to the matrix [5].

Fiber debonding occurs when the fiber separates from the matrix due to cracks that run parallel to the fibers. These cracks break up the chemical bonding that existed between the fiber and adjacent matrix, and create new surfaces. An increase in fracture

toughness is observed with debonding as an intermediate amount of strain energy is released with the creation of new surfaces. Debonding may also increase the critical impact energy of the laminate as a lower interface strength will promote debonding and delamination; in which more elastic strain energy can be released [6].

2.2.1 Delamination

Of the many failure modes that can occur within a composite laminate, one of the most common and pervasive is delamination- "it is an essential issue in the evaluation of composite laminates for durability and damage tolerance" [5, 7]. Matrix cracking, fiber fracture and even local fiber buckling can be seen from a human observer upon their occurrence, delamination though, cannot be seen from the surface of the laminate so external damage inspection can be insufficient in detecting delamination. This is a major weakness of laminated composite structures and a substantial amount of research has been and is still being put into understanding delamination initiation; as well as its subsequent propagation. Because of this concern, aerospace components and structures are designed to handle mechanical strains well below their failure strains during assumed operational loading [8]. This concern is especially true for thin laminates, as the damage has been observed experimentally to occur on the bottom (or opposing) side of the laminate during impact. Whereas for thicker laminates, matrix crushing is more visible on the top (outer) surface and indenting of the laminate from a local impact is visible and more similar to the denting failure mode seen with metals during impact. As previously mentioned, when the various failure modes occur within composites, strain energy is released: when a delamination (or crack) occurs and subsequently propagates, a relatively

large amount of strain energy is released, especially in the case of a ductile and toughened matrix, which absorbs energy via plastic deformation. When fiber fracture coincides with matrix cracking or delamination, a substantial amount of strain energy is released [5].

Plies within a laminate bond to one another by the curing of the matrix constituent, and maintain by the development of interlaminar shear stresses in between plies. Delamination occurs when these interlaminar bonds are broken and the plies are free to move past one another; either in a normal or shearing action. Composites materials with lower interlaminar shear strength (ILSS) are more likely to fail by delamination than materials with a higher ILSS. ILSS is driven by the toughness and ductility of the resin and the chemical bond it induces to bond plies together; hence delamination, ILSS, and fracture toughness in general are matrix driven phenomena.

While it is believed that many factors play a role in a composites fracture toughness, such as; fiber volume fraction, ply orientation, and the tensile strength and elastic modulus of both the matrix and fiber, the dominant factor has been found to be the toughness/ductility of the resin system (matrix) as it plays the dominant role in absorbing energy through plastic deformation and releasing strain energy during the failure process [7]. Several researchers, including Russell and Street [1987] have studied the effect of matrix toughness relative to fracture toughness and found that the interlaminar fracture toughness increased and was greatly affected by the toughening of the resin system within the laminate [7].

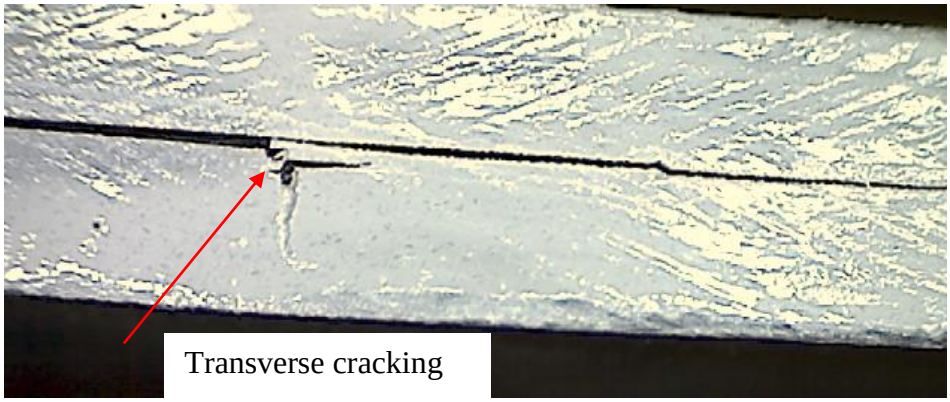

Figure 3 Unidirectional laminate with mid-plane delamination and transverse cracking.

There are many leading causes for the onset of delamination; poor bonding during cure cycle, manufacturing defect/inclusion, low ILSS, impact loading and edge effects. If the cure cycle is not properly achieved then the bonding of the resin in between plies may be insufficient to carry the loads that it was designed for. Likewise, if there exists a defect or inclusion from a manufacturing process or mishandling of the structure, then the onset of delamination, or premature failure in general, is more likely to occur. As previously discussed, a composite material with a lower ILSS will be more susceptible to delamination and a loss of stiffness and damage tolerance of the structure. Composites not suitably designed for impact loading are at a high risk for interlaminar delamination, even low velocity impact, as debonding and delamination can initiate from the impact zone and spread through several plies of the laminate. Design engineers and composite researchers in the Aerospace industry still invest in understanding delamination and predicting how they initiate and propagate.

2.2.2 Composite Failure Analysis

Several composite laminae failure theories have been developed since the 1970's and 80's that predict the onset of damage within composites. Such failure theories include Christensen, Hashin, Tsai-Wu and Tsai-Hill (also known as "Maximum-Work Theory"). These theories attempt to predict the strength of a laminae and can be applied for biaxial and shear loading. The Hashin criterion is unique in that it decomposes composite failure into four sub-categories: compressive and tensile failure of the matrix and fiber respectively for a 2D state. [9]. These failure theories though are unable to properly model delamination for two key reasons: 1) They are 2D laminae failure theories, thus are unable to account for through thickness effects such as the interface between two plies (or edge effects), 2) They only predict the onset of damage, and not it's propagation (such as crack growth). Hence, for the purpose of understanding delamination and it's propagation in terms of fracture toughness, a different method of analysis is needed to capture the effects of interlaminar delamination. This method is a subset of structural analysis and is known as Fracture Mechanics. It is important to note that the before mentioned theories (and the like) are semi-empirical in nature; all of them must be supported by experimental testing to validate the theories' capacity to accurately predict damage onset.

2.3 Griffith Fracture Approach

Fracture mechanics is unique as compared to traditional structural analytical methods in that flaws within a structure are assumed to be present. The objective is to determine the structures' resistance to fracture via calculating critical flaw (crack) size, critical applied stress, or the number of cycles permitted before fracture by fatigue. Unlike fracture mechanics, the use of the isotropic constitutive relation, beam theory, classical laminate theory, etc. all assume a virgin material in which no flaws/cracks exist.

Alan Arnold Griffith is considered the first in developing the field of fracture mechanics and developed his criteria for brittle fracture by the 1920's. Griffith was an aeronautical engineer who studied brittle materials such as rocks and glass. Despite being initially scrutinized for his work, his findings and theoretical developments in fracture became widely used by the 1940's & 50's for aluminum and steel structures such as airplanes and ships during the times of war. His work was continued and further developed by prominent engineers such as Irwin, Orowan, Dugdale, Rivlin and Rice. Griffith's famous fracture criteria, along with other fundamental and relevant practices within fracture mechanics (relative to this thesis), will be developed in the following sections.

In order to understand crack propagation, and develop a criterion for crack growth, consider an infinite plate with uniform stress loading σ and a through thickness crack of the length 2a, as seen in Figure 4.

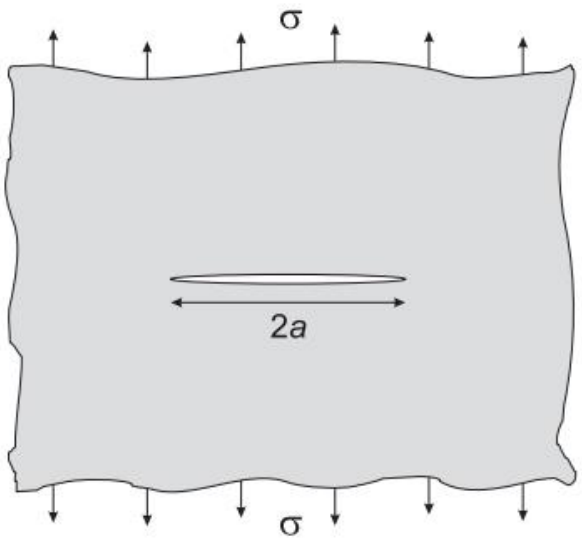

Figure 4 Through-thickness crack of infinite wide plate [10].

Using the first law of Thermodynamics and applying an energy balance to the plate:

$$U = U_o + U_a + U_\gamma - F \tag{1}$$

Where U is the total energy of the plate, U_o is the energy of the plate before introducing a crack, U_a is the energy reduction from introducing the crack, U_γ is the surface energy associated with introducing the crack, and F "is the work performed by the loading system during the introduction of the crack" [10]. F is assumed to be zero with fixed grips, and U_a & U_γ are defined respectively as:

$$U_a = -\frac{\pi\sigma^2 a^2}{E} \tag{2}$$

$$U_\gamma = 4a\gamma_e \tag{3}$$

Equations (13) & (14) into equation (12) giving

$$U = U_o - \frac{\pi\sigma^2 a^2}{E} + 4a\gamma_e \tag{4}$$

"Following Griffith, crack extension will occur when U decreases. In order to formulate a criterion for crack extension, we consider an increase of the crack length d(2a). Since U_o is constant, it will not change and $dU_o/d(2a)$ is zero. Also, since no work is done by the loading system, the driving force for crack extension can be delivered only by the decrease in elastic energy dU_a due to the crack length increase d(2a). The crack will extend when the available energy dU_a is larger than the energy required dU_γ" [10]. A graphical representation of the latter is seen below in Figure 5.

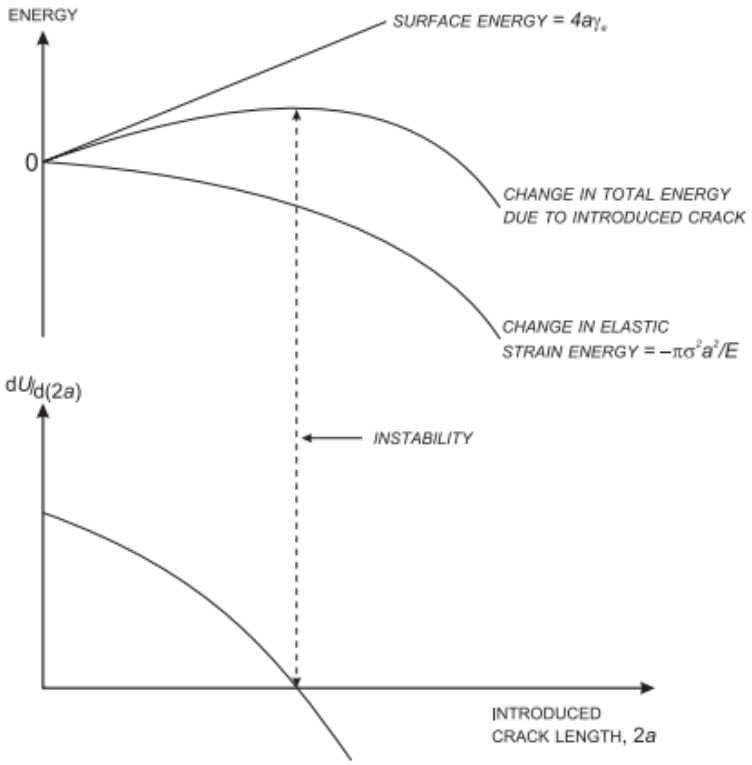

Figure 5 "Energy balance for a small crack in a large plate loaded under fixed grip conditions" [10] .

Taking $\frac{dU}{d(2a)} < 0$ of equation (15) gives

$$\frac{\pi\sigma^2 a}{E} > 2\gamma_e \tag{5}$$

Rearranging,

$$\sigma\sqrt{\pi a} > \sqrt{2E\gamma_e} \tag{6}$$

Equation (17) is the crack extension criteria for brittle materials; the left-hand-side is comprised of system conditions σ and a whereas the terms on the right-hand-side are material properties and hence, constant. E is the Young's Modulus of the material and γ_e is the surface energy of the material which represents the energy required at an atomic level to break the atomic bonds and create new surfaces through the process of crack extension. If the product of the left-hand system properties exceeds the product of the material properties on the right-hand-side, then crack growth will occur and will do so rapidly. "When the elastic energy release due to a potential increment of crack growth, d(2a), outweighs the demand for surface energy for the same crack growth, the introduction of a crack will lead to its unstable propagation" [10]. In other words, more energy is available to the system (per loading conditions & flaw), then is required to extend the crack via the necessary surface energy needed to create new surfaces- hence unstable crack growth. Stable crack growth can be and is obtained in real situations, such as fatigue loading, but the energy balance approach is not able to address such cases [10]. Simply, when $dU/d(2a) \leq 0$, then unstable crack extension will occur.

2.4 Stress Intensity

The left-hand-side of equation (17) has been defined as the *stress intensity factor* and is denoted by the variable K.

$$K = \sigma\sqrt{\pi a} \tag{7}$$

"K is a quantity which gives the magnitude of the elastic stress field" [10] and has units of $Mpa\sqrt{m}$ or $ksi\sqrt{in}$. K_c is the critical stress intensity factor in which above it, fracture will propagate; K_c is equal to $\sqrt{2E\gamma_e}$ and can be found experimentally. See [10] for details on experimental methods for determining K_c and fracture mechanics in general. For mode I loading, K_c is also deemed K_{IC} and can thought of as either of the two following conditions:

$$\mathrm{K_{IC}} = \sigma_c\sqrt{\pi a} \tag{8}$$

In which the critical stress, σ_c, is found for a given crack size, or

$$\mathrm{K_{IC}} = \sigma\sqrt{\pi a_c} \tag{9}$$

Where the critical crack size, a_c, is found for a given applied stress.

It is important to note that the K_{IC} developed above is for an infinite wide plate- in general:

$$\mathrm{K_c} = \sigma\sqrt{\pi a}\ \left\{f\left(\frac{a}{W}\right)\right\} \tag{10}$$

Where W is the width of the plate or specimen. If the crack length is of the same order of magnitude of the width, then the stress intensity factor will be a function of the ratio (a/W). This is crucial for design and analysis purposes of a structure because equation (21) implies that K_c is expected to be different for two common engineering analytical practices; both of which use different assumptions pertaining to their respective analytical methods. These are known as plane stress and plane strain: the differences in stress intensity for plane stress & plane strain have been determined experimentally and are seen in Figure 6.

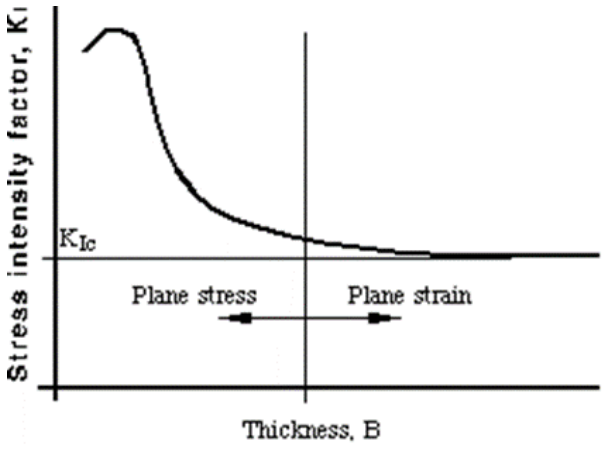

Figure 6 Stress intensity factor as function of specimen thickness [11].

Due to the extreme variation in stress intensity factor via thickness, K_{IC} for plane strain is conventionally accepted as the standard for stress intensity factor since it is a more conservative estimate. As seen in Figure 6, once a critical specimen thickness is reached for plane strain, K_{IC} will remain constant. Hence, when experimentally determining K_C (for any mode), caution must be taken to ensure that the test specimen is in a state of plane strain.

2.5 Modes of Fracture

The type, or mode of fracture that has been discussed so far is mode I behavior: two cracked surfaces that open normal to one another as crack growth occurs. This is the case for the through thickness crack of the infinite plate in Figure 4. In reality, there are three modes of fracture that occur; mode I- normal or opening mode, mode II- the cracked surfaces shear past one another in the plane of the crack & crack movement (consider transverse loading on a simply supported beam), and mode III- a tearing mode where the crack surfaces slide past one another out of plane- orthogonally relative to crack propagation. These are considered to be "pure" modes of fracture as they occur independently of the other modes; and are displayed in Figure 7.

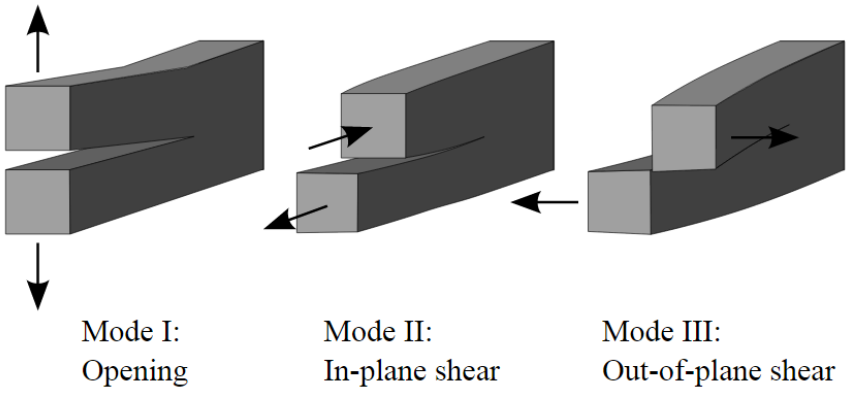

Figure 7 Three pure modes of fracture [12].

Fracture is not limited to pure mode behavior though, mixed-mode behavior can and does occur in real structures and can be tested experimentally and simulated via finite element modeling.

2.6 Strain Energy Release Rate

By referring to the left hand side of equation (16), another important and useful expression with fracture mechanics testing can be utilized: Irwin designated this as the energy release rate, G, and represents "the energy per unit new crack area that is available for infinitesimal crack extension" [10]. Since U represents the total strain energy of the infinite plate in equation (12), G is also called the *strain energy release rate* or SERR. For the infinite plate, G is given by

$$G = \frac{\pi\sigma^2 a}{E} \tag{11}$$

In general, for a finite plate of width B, the SERR is defined to be

$$G = -\frac{1}{B}\frac{dU}{da} \tag{12}$$

For plane strain, the critical G and K values are related by the following expression.

$$G_c = \frac{K_c^2\,(1-\nu^2)}{E} \tag{13}$$

For experimental purposes, it is more convenient to express the SERR in terms of a test specimen's compliance as a function of crack length. For instance, a simply supported beam will be more compliant (less stiff) as the crack length increases. The well-known Irwin-Kies expression is given below and expresses fracture energy (G) in terms of the compliance of the test specimen. See Josh Smith [1] for a complete derivation of the Irwin-Kies expression.

$$G = \frac{P^2}{2}\frac{dC}{da} \tag{14}$$

Where C is the compliance of the system and changes with crack length. This is the general expression for SERR and can be used for all fracture mode behavior, including mixed-mode behavior. It is commonly used for testing purposes to obtain the fracture energy of materials that are orthotropic such as composite laminates. The relevant compliance function w.r.t what test is being performed, can be inserted into equation (24) to obtain the SERR for that particular mode of fracture for a given material.

2.7 Crack Tip Plasticity

The LEFM theory introduced has assumed that no yielding occurs at the crack tip, and that the stress is theoretically infinite at the tip of the crack. This stress singularity obviously does not occur in reality, so the 3D stress equations obtained from the theory of elasticity must be adjusted to reconcile the stress singularity and to account for the plastic zone that occurs ahead of the crack tip. This phenomena is seen in Figure 8.

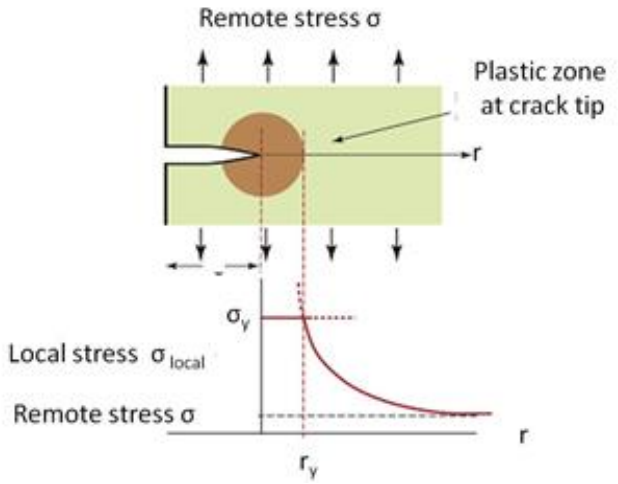

Figure 8 "Plastic yield zone at the crack tip" [13].

Since the 1940's, several pioneers within the fracture mechanics community have proposed models to estimate the length of the plastic zone- defined as r_y. One of the most basic was proposed by Irwin:

$$r_y = \frac{1}{2\pi}\left(\frac{K}{C\sigma_{ys}}\right)^2 \tag{15}$$

Where σ_{ys} is the yield strength of the material and C is a constant that varies on specimen thickness per the phenomenon previously discussed and seen in Figure 6. For plane stress, C is 1, and for plane strain C is assumed to be 1.7 [10].

Because of the plastic yielding that occurs at the crack tip, the size of the crack can be treated as though it is longer then it really is; or in other words- due to plastic yielding the crack behaves as though it is longer than the actual flaw size. To account for this plastic zone, the stress intensity factor is adjusted by adding the plastic zone length to the crack length in order to get an effective flaw size, as defined below in equation (27) for mode I.

$$K_1 = \sigma\sqrt{\pi(a + r_y)} \tag{16}$$

Substituting equation (26) into equation (27), one obtains

$$K_1 = \frac{\sigma\sqrt{\pi a}}{\sqrt{1 - \frac{1}{2}\left(\frac{\sigma}{\sigma_{ys}}\right)^2}} \tag{17}$$

Equation (28) is an approximate for brittle materials that have small crack tip plasticity. If the material is ductile or the plastic zone ahead of the crack tip is large relative to the specimen characteristic length (thickness or width, etc.) then this approximation breaks down as it can only be used for Linear Elastic Fracture Mechanics (LEFM): what has been presented thus far.

CHAPTER 3: MODE I & MODE II EXPERIMENTAL FRACTURE TESTING

3.1 Introduction

Fracture testing of composites has been performed as early as the 1970's and has become generally accepted for characterizing the fracture toughness of composite materials. Initially though, composite fracture testing was met with much scrutiny; some of the issues regarding early fracture testing was its lack of adherence to theories previously adopted for metals, as well as a lack of consistent and replicable test results. As testing methods have improved, and a more accepted theoretical approach has been adapted, the field of composite fracture testing has vastly improved and grown over the decades [14]. To maintain consistency and uniformity within testing, standardized testing procedures have been established by major industry level organizations, for metallic and non-metallic materials. Such non-metallic materials include composite materials and are performed for the different modes of fracture: pure and mixed-mode behavior respectively. The focus of this thesis will be fracture testing of composite materials, particularly, continuous fiber unidirectional composite laminates. Some of the main testing standard organizations include ISO (International Organization for Standardization), JIS (Japanese Industrial Standards) and ASTM (American Society for Testing and Materials). The testing standards followed in this thesis will be that of the ASTM and its adopted methods for testing of the mode I & mode II fracture toughness of unidirectional composite laminates. It is important to note- though several legitimate and nationally accepted testing standards exist, there are differences in the fracture tests performed and their corresponding procedures; indicating that there is not a complete

consensus within the materials' community on testing methods and setup. See A.J Brunner et al. for a comparison on several composite fracture testing methods [15].

For decades, fracture testing has been performed for pure mode and mixed-mode behavior, with several receiving acceptance as standardized testing procedures. Some tests though, while still accepted, are in dispute, as well as others that have yet to be certified. To this date, ASTM has adopted three standards for fracture testing of composites; ASTM D5528 (mode I), ASTM D7905 (mode II) and ASTM D6671 (mixed mode I/II). The first adopted standard was ASTM D5528 and done so in 1994; it has since then been revised several times. Despite Mode II testing being performed since the 1980's by several organizations and with different test procedures, there still has been much dispute over which methods should be accepted and if they are accurate & repeatable [15, 16]. Because of this, ASTM D7905 was not accepted until 2014 but is still in dispute today over its validity as the "best" testing method, see [16] for a comparison of the mode II test procedures, and subsequent pros and cons of each method. ASTM D6671 was adopted in 2001 after being proposed by Reeder and Crews; despite the test fixture being criticized for its' cost and complexity, the D6771 test procedure is well accepted [17]. Other mixed mode behavior interactions (I/III & II/III) have been studied [15, 18] but no testing standards have been established. Additionally, although mode III fracture testing has been performed and studied for several decades, ASTM has yet to adopt a testing standard. Despite an industry standard though, many new developments have been made in characterizing mode III behavior and can be reviewed in [19, 20, 21, 22]. A summary of testing methods used in this thesis can be seen in Appendix D; ASTM D5528 & D7905 can be found in [23, 24].

3.2 Mode I DCB Testing: ASTM D5528

Before the common practice of performing fracture toughness experiments for composite materials, the most prevalent test for mode I fracture strength was the the compact tension (CT). The CT test is mainly suitable for isotropic materials, but can also be used for “some types of composite materials that have limited orthotropy, including nanoparticle, particulate, whisker and short-fiber composites. For highly orthotropic materials (highly directional reinforced) composites”, such as unidirectional fiber reinforced polymer matrix composites, ASTM D5528 should be used [23].

ASTM D5528 relies on the use of a double cantilever beam (DCB) test specimen, in which normal (opening) loading is applied with pure mode I fracture occurring during crack propagation. Test setup and loading fixtures can be seen below Figure 9 & Figure 10. See Josh Smith [1] for a more complete development of ASTM D5528 theory, testing process and DCB literature background.

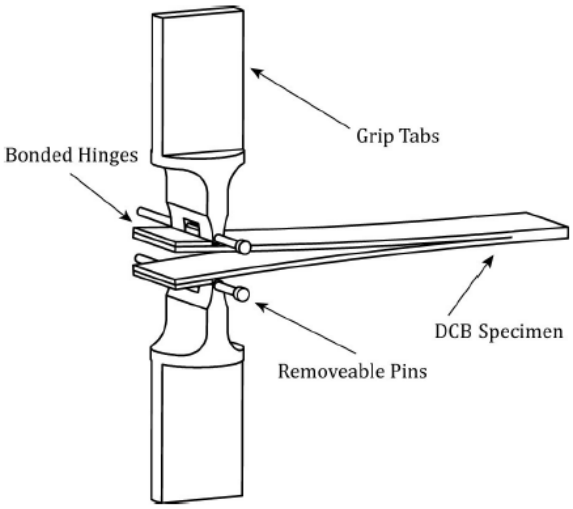

Figure 9 Test fixtures and specimen for double cantilever beam (DCB) [1].

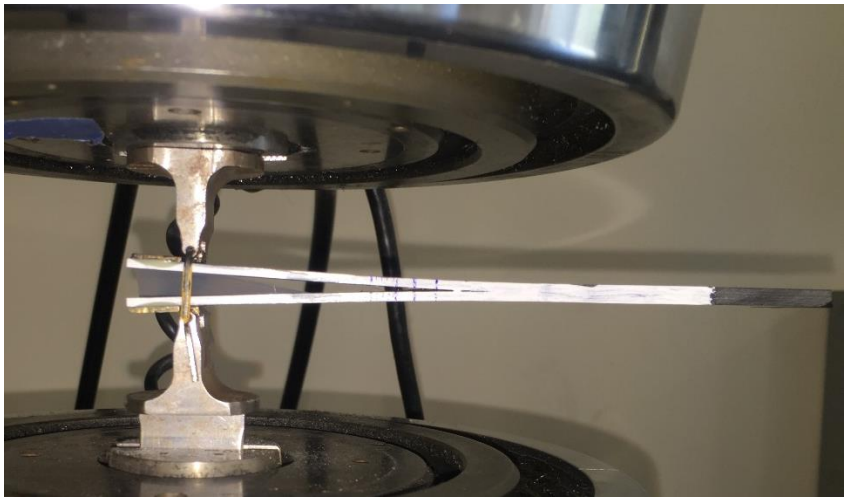

Figure 10 Instron loading of DCB specimen with bonded fixtures.

3.2.1 Mode I SERR

ASTM D5528 calculates the mode I fracture energy by using theoretical principles from Linear Elastic Fracture Mechanics (LEFM). As seen in section 2.8, the Irwin-Kies expression for the SERR for mode I fracture is given by

$$G_I = \frac{P^2}{2B}\frac{dC}{da} \tag{18}$$

Several SERR calculation methods are presented within the ASTM standard including; Beam Theory (BT), Modified Beam Theory (MBT), Compliance Calibration (CC) & Modified Compliance Calibration (MCC) [24]. BT will be presented and used herein, for details pertaining to the other methods, see Josh Smith [1]. Using the compliance of a cantilever beam given by Beam Theory, and equation (29), the mode I SERR becomes

$$G_I = \frac{3P\delta}{2ba} \tag{19}$$

Where P is the max load reached during loading and δ is the opening displacement of the DCB specimen that occurs at the before-mentioned load P. The initial delamination length is given as a, and the specimen width, b. These are seen in Figure 11 below.

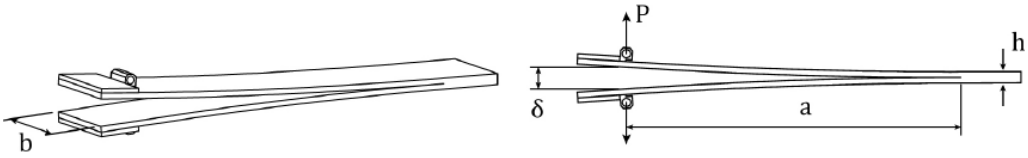

Figure 11 "DCB test specimen dimensions" [1].

3.2.2 DCB Results

Three composite laminate beams were tested to obtain a rough estimate of the mode I fracture toughness of M46J/TC250 uni-directional tape. The uni-directional pre-preg was donated to Cal Poly by SpaceX with an off-shelf expiration date of 2013. One specimen had a built-in delamination using mold release; the other two specimens contained a PTFE film insert to create the delamination. Non-pre-crack and pre-cracked tests were performed on all DCB laminates. Specimen dimensions are found in Table 1.

Table 1 Dimensions of DCB specimens.

Specimen ID	Length (in)	Width (in)	Thickness (in)
MR-S1	5.12	.47	.17
TE-S1	6.33	.51	.16
TE-S2	6.32	.52	.16

Table 2 Fracture energy [G_{IC}] of DCB specimens; non pre-cracked test

Specimen ID	NPC G_{IC} (Psi-in)
MR-S1	N/A
TE-S1	0.56
TE-S2	0.95

Table 3 Fracture energy [G_{IC}] of DCB specimens; pre-cracked test.

Specimen ID	PC G_{IC} (Psi-in)
MR-S1	0.99
TE-S1	0.50
TE-S2	1.50*

A NPC fracture energy was not obtained for MR-S1 due to the abnormally high max load that was achieved during initial loading. An extensive research into previous mode I testing date revealed that most uni-directional DCB specimens reach a critical load in the range of 15-40 pounds, rarely over 50. MR-S1 though, exceeded 115 pounds. It is believed that the mold release used did not create a perfect built-in delamination, such that patches of resin had bonded in the anticipated delamination region, creating a large increase in toughness. This strength increase is artificial and is not considered to be the critical mode I fracture toughness of the laminate/matrix. The load-displacement curve of specimens MR-S1 and TE-S2 can be seen in Figure 12 and Figure 13 respectively. It is important to note though that once the “co-cured bonding strength” of

MR-S1 reached critical load, the loads attained during steady state fracture were virtually identical for the NPC and PC tests.

Noticeable fiber-bridging was observed in specimen TE-S2. Fiber-bridging is when fibers remain attached to the top & bottom sub-laminates during opening displacement of the DCB test. Fiber-briding is mostly predominant in uni-directional layups such as $[0]_n$ and is accompanied by an artificial increase in G_{IC}, which explains why the G_{IC} for TE-S2 was triple that of it's counterpart TE-S2 (made from same batch/insert method). The increase in strength is deemed artificial because the fibers carry mechanical load during the bridging process; providing an increase in resistance to displacement (i.e stiffness), hence leading to a false (artificial) value of fracture toughness which relies on the strength of the matrix. Examples of fiber-bridging are found in Figure 14 and Figure 15.

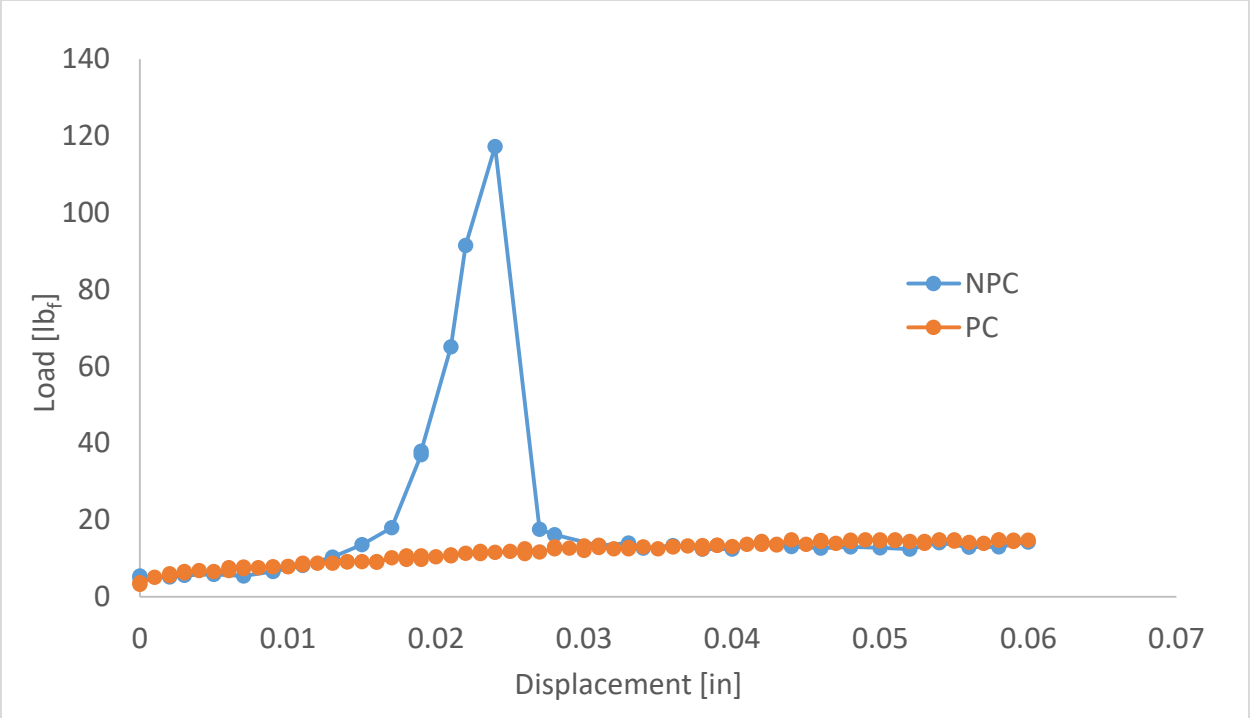

Figure 12 DCB P-δ curve of non-pre-cracked & pre-cracked test; specimen MR-S1.

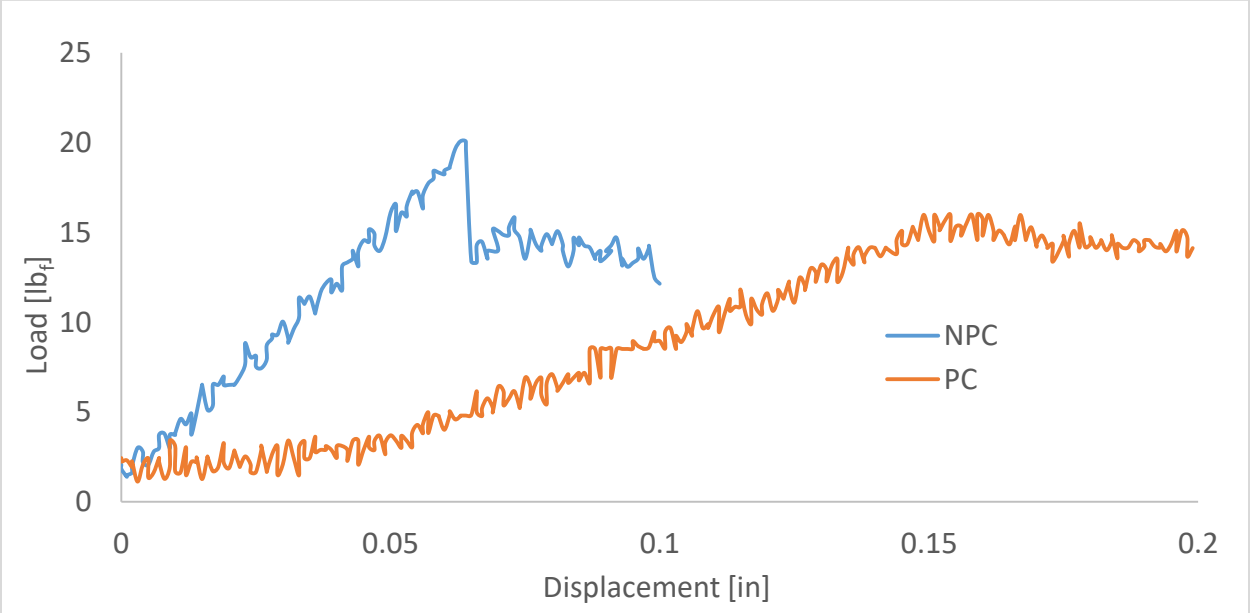

Figure 13 DCB P-δ curve of non-pre-cracked & pre-cracked test; specimen TE-S2.

TE-S2 had a higher fracture energy for the PC test than the NPC respectively, the artificial increase in fracture energy is best explained by fiber-bridging that occurred during steady state fracture; as shown in Figure 15. Specimen MR-S1 also experienced fiber-bridging but in a different manner. As seen in Figure 14, the fiber-bridging observed was done so by large ligaments of an entire ply bridging across the top and bottom sub-laminates; whereas the fiber-bridging that occurred with TE-S2 (PC) was seen as several individual fibers bridging between the sub-laminates.

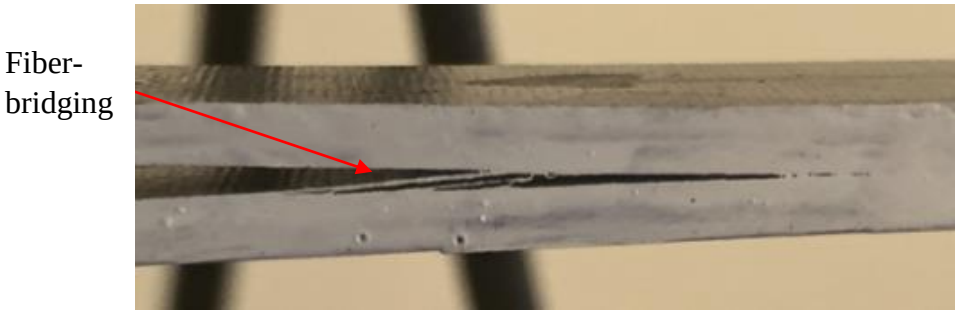

Figure 14 Fiber-bridging of DCB specimen; mold release delamination- PC test.

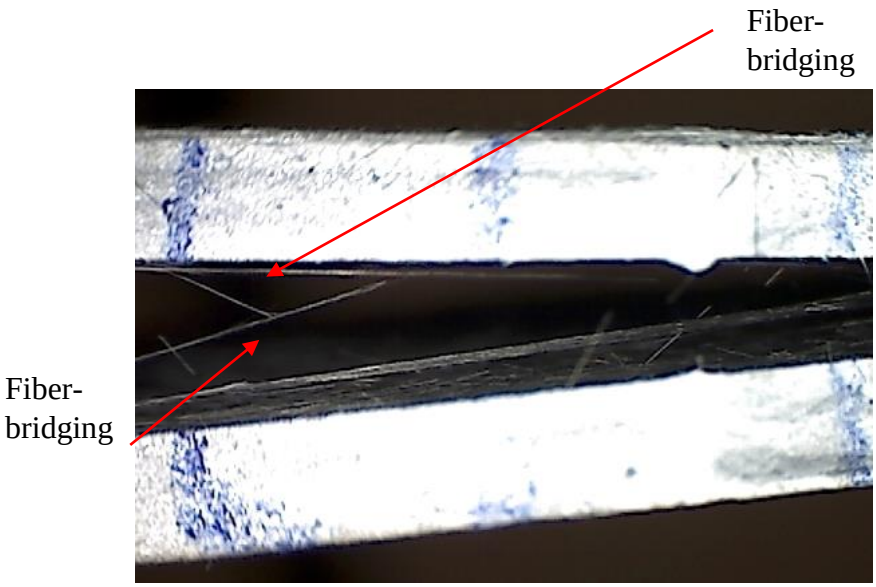

Figure 15 Fiber-bridging of DCB specimen; PTFE delamination- PC test.

Nearly identical loads were reached during steady state fracture for both NPC & PC tests from TE-S2; indicating that the steady state fracture toughness values are independent of which test is being performed (NPC vs. PC). While the PC initiation fracture energy is 60% higher than the NPC fracture energy (due to fiber-bridging), the PC specimen was 2.55 times more compliant during loading in the initial elastic region- suggesting that root compliance plays a larger role in fracture for a PC specimen than crack initiation as observed for the NPC. A possible explanation for the difference in root compliance is that a small neat resin pocket is developed at the front of the PTFE insert; this pocket can provide an increase in stiffness as neat resin resists against the opening displacement as it absorbs energy via plastic deformation. Upon initial crack propagation, the crack root becomes more compliant as yielding ahead of the crack tip occurs (process zone) as the crack is able to travel through the interface in-between and alongside the fibers.

Fiber bridging was not as prevalent for TE-S1 as the other two specimens. Despite the decreased amount of fiber bridging, the large variance of fracture energy values between TE-S1 and TE-S2. Considering that both of the latter specimens were from the same batch of manufactured parts, the discrepancy between TE-S1 & TE-S2 G_{IC} value is inconclusive.

3.3 Mode II ENF Testing: ASTM D7905

To this date ASTM has accepted the End-Notched-Fixture (ENF) as the test specimen to be used for mode II fracture of unidirectional composite laminates. This specimen (ENF) is also referred to as the 3ENF because a 3-point-bend test fixture is used to induce the shear loading of the specimen: 3ENF & ENF will be used interchangeably. The test specimen and fixture can be seen in Figure 16 & Figure 17. Per ASTM D7905, "This method is limited to use with composites consisting of unidirectional carbon-fiber and glass-fiber reinforced laminates. This limited scope reflects the experience gained in round robin testing. This test method may prove useful for other types and classes of composite materials; however, certain interferences have been noted" [25].

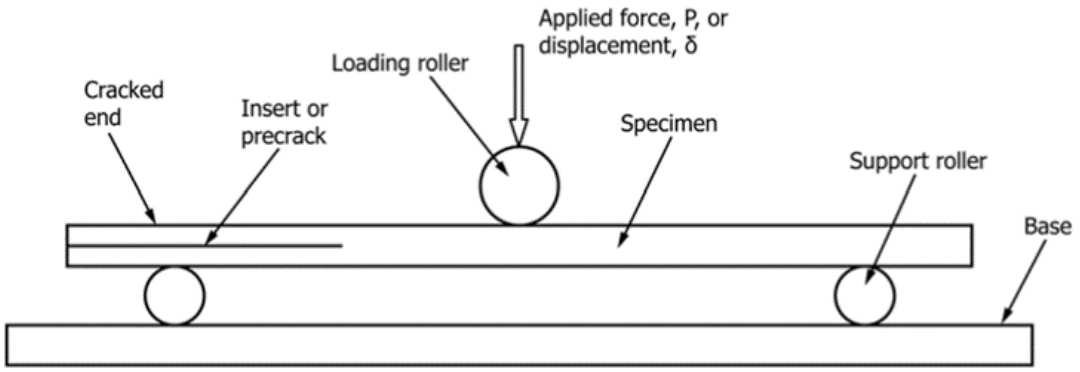

Figure 16 ENF Test Fixture; ASTM D 7905 testing procedure [25].

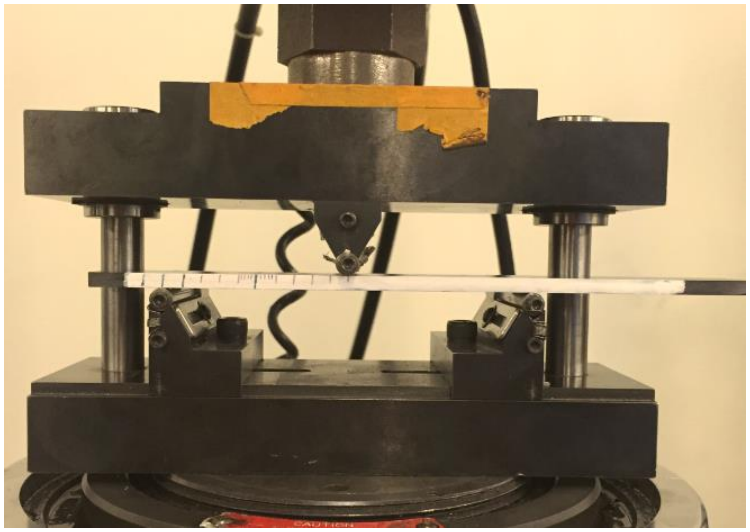

Figure 17 Cal Poly ENF test fixture.

The loading of the ENF is idealized as a simply supported beam with a point load located at half the span, as seen below in Figure 18- along with the shear and moment diagrams of said loading. The transverse shear stress induced in the plane of the crack increases as the top roller force steadily increases from the constant displacement loading. Once a critical load is reached, the crack will extend in the direction of the plane of the crack front. If the loading is uniform and the laminate symmetric, then pure mode II fracture will occur. The ENF test is simple to set up and perform, but unstable crack propagation is of a major concern. This is an issue considering data reduction methods because they require recording of the crack length during fracture testing; and monitoring crack growth for the ENF has proved difficult in the past [26]. “The ENF test is the most widely used mode II test, but its inherent instability is a serious drawback” [16]; stable crack propagation is only expected when the crack length is at least 70% of the total span

length. This may be achieved during PC testing, but will not occur during NPC per ASTM D7905, hence unstable crack propagation will occur during the initial NPC test which produces the pre-crack length for the PC test. This could possibly be a reason for why the ENF test has been scrutinized during its use and now standardization.

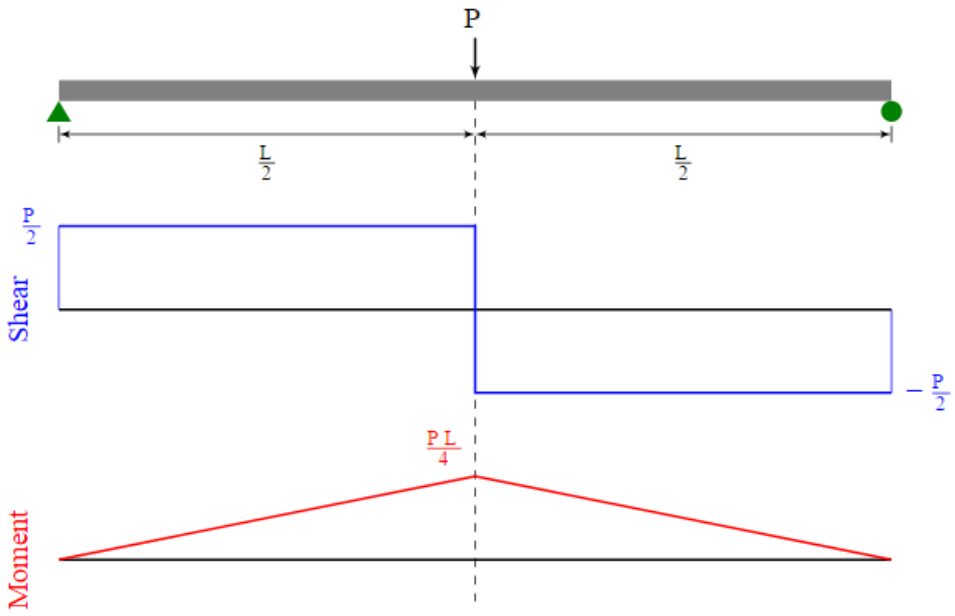

Figure 18 "Shear and moment diagram for a simply supported beam with a concentrated load at mid-span." [27].

3.3.1 ENF SERR

ASTM D 7905 relies on the Compliance Calibration (CC) method in order to calculate G_{II}; in which the compliance of the specimen is a function of the crack length. In other words- as the crack length within the span increases, the compliance of the ENF test specimen also increases due to the influence of the crack on the beam's stiffness. ENF configuration and specimen for CC is seen in Figure 19.

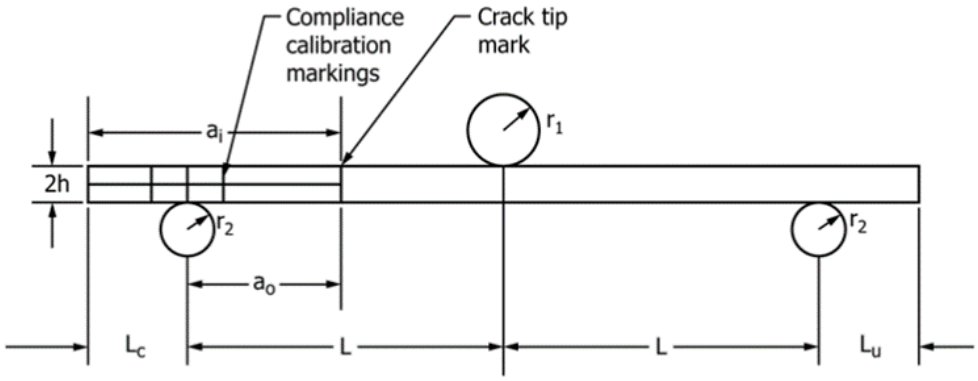

Figure 19 ENF Specimen and Dimensions [25].

Using the Irwin-Kies expression for mode II, one obtains

$$G_{II} = \frac{P^2}{2B}\frac{dC}{da} \tag{20}$$

In which a compliance function for the ENF specimen is assumed to be [25]

$$C = A + ma^3 \tag{21}$$

Where a is the crack length at each respective CC mark is, m is the slope of the curve-fit of compliance vs. crack length, and A is the intercept. A and m are both obtained from regression analysis: the curve-fit obtained is expected to be a linear fit (as to obtain the slope m) and has been observed throughout mode II fracture testing of past ENF specimens [16, 26].

With equation (32) into equation (29), the critical fracture energy for mode II (ENF) becomes

$$G_{II} = \frac{3mP_{MAX}^2 a_O^2}{2B} \tag{22}$$

Where a_O is the initial delamination length and P_{max} is the max load reached during loading, which occurs at initial crack propagation. Equation (33) is the NPC mode II fracture toughness; see ASTM D7905 [25] for more on PC testing and analysis.

3.3.2 ENF Results

Twelve specimens were tested per ASTM D7905 standards, all with mold release built-in delamination's. No mode II fracture toughness's were obtained because all specimens exhibited a unique phenomenon in which the specimen compliance did not change when the crack length within the span was changed, as presumed with Compliance Calibration. This suggests that the mold release did not create a suitable built-in delamination and that sufficient matrix bonding had occurred at the mid-plane interface such that the two sub-laminates behaved as one; hence no variation in beam compliance for a given span length and no real crack. An illustration of this behavior can be seen in.

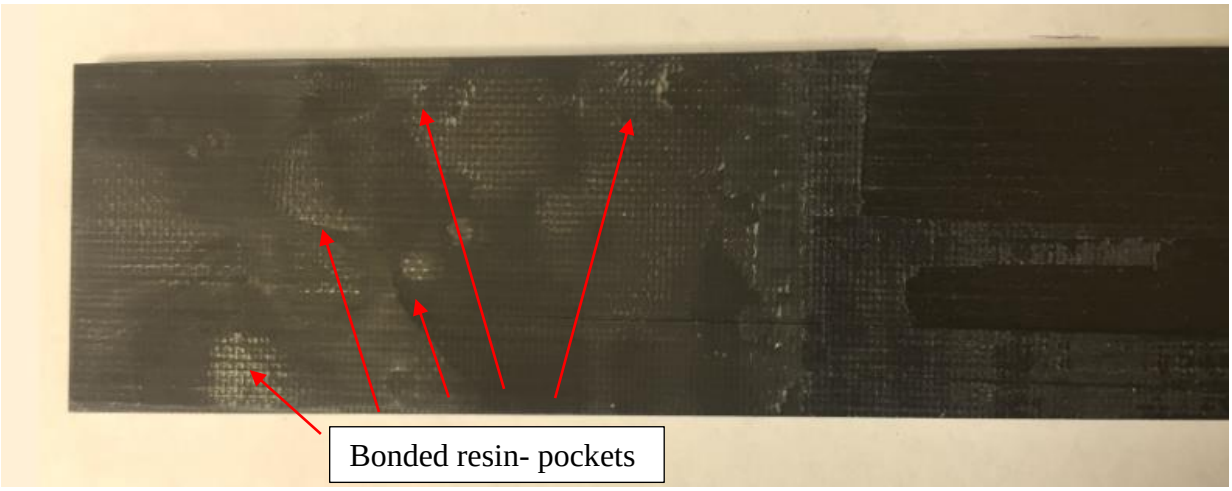

Figure 20 Top view of mid-plane ply of 3ENF specimen; mold release delamination.

The stiffness, and conversely the compliance, of the ENF beams did not change when the crack length contained within the span varied. This leads to a slope, m, of zero; which suggests (per CC theory) that the specimen has zero fracture toughness.

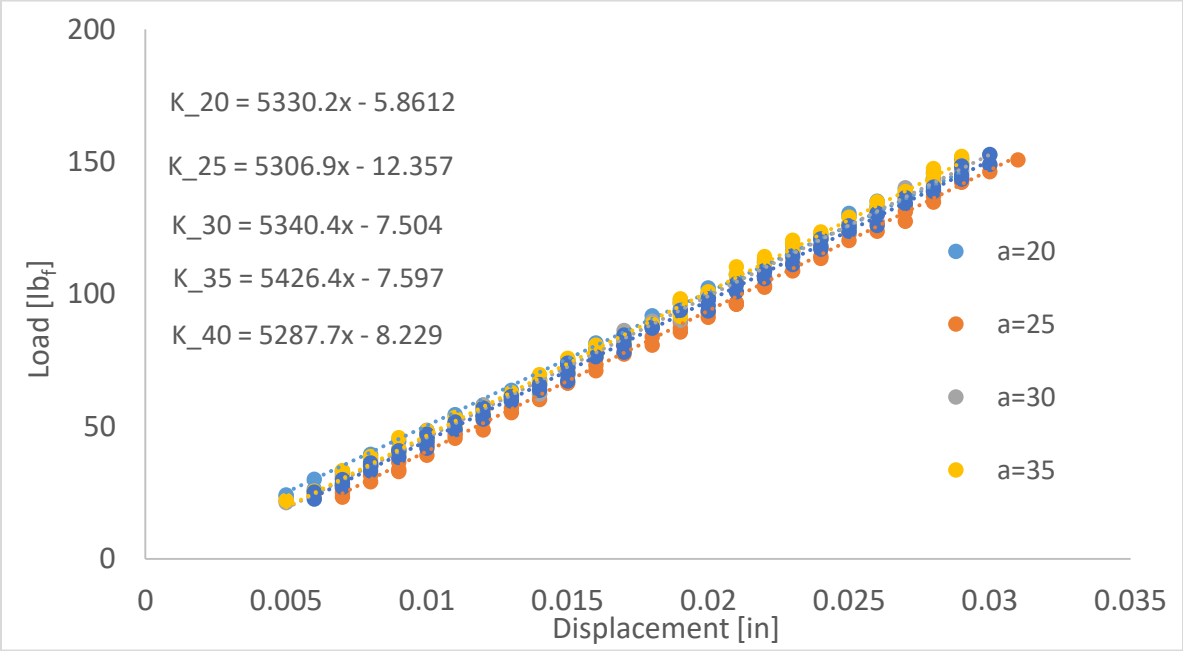

Figure 21 P-δ of ENF test; ASTM D 7905

To explain this anomaly, it was hypothesized that, like the mode I specimens, the mold release did not create a perfect built in delamination, hence when CC was performed, the beam essentially behaved as if there was not a delamination that would've lead to a variance of stiffness/compliance when the crack length varied. Once concluding mode II fracture testing (3ENF), several specimens were examined at the laminate mid-plane to investigate the effectiveness of the mold release to create the delamination. Pockets of "potential bonding" can be seen in; these pockets are believed to be the cause of constant stiffness as the top and bottom sub- laminates are sufficiently bonded during CC and did not cause the compliance to be a function of crack length. It is inconclusive

as to whether the quality of the mold release, or the innate use of a mold release, is the underlying cause for such unique and unexpected behavior.

3.3.3 Mode II 4ENF Testing

The 4ENF test was originally one of the candidates for ASTM adoption for G_{IIC}, but the ENF test was chosen and certified in 2014 [25]. One of the concerns around the 4ENF was the inconsistency of results obtained by several testing centers prior to 2000. During that study, only JIS (who has accepted the 4ENF as their mode II fracture testing standard) reported consistent results. Additionally, frictional effects were of concern as the error associated with friction was found to be greater for the 4ENF than the ENF test specimen. Davidson and Schuecker [28] studied the 4ENF fracture test and with the use of finite element analysis, discovered that though friction did influence the fracture toughness results, as seen by an increase in delamination resistance, the error was still acceptably small [29]. At the time of the international round robin mode II fracture tests [16], the 4ENF had not been commonly used in research practice; this was seen as a disadvantage for selecting the 4ENF [16]. The 4ENF has been studied more extensively since then and is recognized as a suitable test for acquiring G_{IIC} for uni-directional composite laminates [29, 30, 31]. 4ENF test fixture and specimen configuration can be seen in Figure 22 & Figure 23.

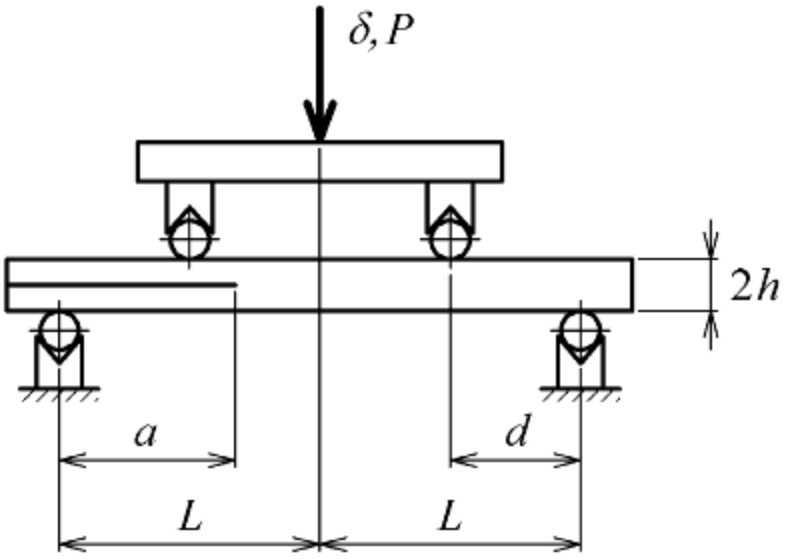

Figure 22 Test fixture & schematic for 4ENF mode II test [26].

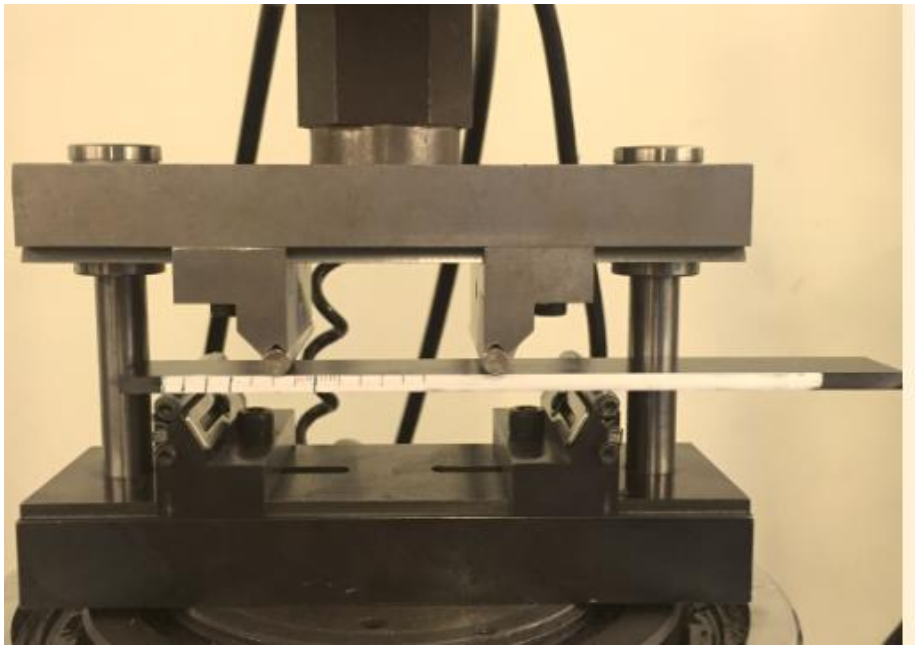

Figure 23 4ENF test specimen & fixture.

3.3.4 4ENF SERR

Performing the four-point bend test is simpler and quicker than the three-point bend set up used by ASTM D7905. Unlike ASTM D7905, fracture energy can be calculated by either compliance method or beam theory. The 4ENF test has several advantages as compared to the ENF: 1) compliance calibration need not be performed as the compliance method used for 4ENF fracture energy analysis only requires one compliance value which occurs during the actual test. 2) Crack length does need to be recorded during the test, only the initial delamination length needs to be known. 3) Stable crack propagation can occur unconditionally, whereas ENF must have the crack length be 70% of the overall span to ensure stable crack propagation.

The assumed compliance function for the 4ENF is given in equation (34) [16].

$$C = D + ma \tag{23}$$

Where D is the intercept, m is the slope of the compliance vs. crack length linear curve-fit, and a is the initial delamination length. With equation (34) into the Irwin-Kies relationship, the fracture energy per 4ENF becomes

$$G_{II} = \frac{P_{max}^2 m}{2b} \tag{24}$$

With Beam Theory, the compliance for a 4ENF specimen is given as [32]

$$C = \frac{L^3}{32E_{11}bh^3}\left(1 + \frac{9a}{L}\right) \tag{25}$$

Equation (36) into Irwin-Kies yields G_{IIC} as

$$G_{II} = \frac{9P_{max}^2 d^2}{16E_{11}b^2h^3} \tag{26}$$

Beam Theory was used for calculating G_{IIC} for all 4ENF specimens.

3.3.5 4ENF Results

Overall six 4ENF specimens were tested; four with the mold release delamination method, and the remaining two with a PTFE insert. Equation (37) was used to calculate G_{IIC}, max load and fracture toughness results are given in Table 4.

.

Table 4 Max load and mode II fracture energy for Mold Release 4ENF specimens.

Specimen ID	P_max (lb_f)	G_IIC (Psi-in)
4E-MR-S1	395	1.92
4E-MR-S2	469	2.71
4E-MR-S3	444	2.43
4E-MR-S4	422	2.19
AVG.	**433**	**2.32**

Table 5 Max load and mode II fracture energy for PTFE 4ENF specimens.

Specimen ID	P_max (lb_f)	G_IIC (Psi-in)
4E-TE-S1	467	2.52
4E-TE-S2	424	2.07
AVG.	**445**	**2.29**

As seen in Table 4 & Table 5, good agreement is obtained between the mold release and PTFE specimens for the 4ENF fracture test. A sample size standard deviation was calculated to be .34 Psi-in for the MR specimens; considering the presence of matrix degradation seen in the pre-preg, as the well inconsistency that can occur during composite fracture testing- the STD value seems reasonable.

Stable crack propagation was observed in most 4ENF specimens (both MR & PTFE) in contrast to the ENF where no stable crack propagation occurred. As noted by previous researchers, the 4ENF specimen can experience excessive compliance during loading which can lead to calculation error from geometric and loading nonlinearities. The PTFE 4ENF specimens showed good agreement with the MR 4ENF counterparts and gave more conservative values than the MR specimens; though more 4ENF testing is recommended to compare. The 4ENF was simple to perform and did not require recording of the crack size during loading, or initial compliance calibration. If rough, or "ballpark" estimates of G_{IIC} are desired, than it is recommended that the 4ENF test be performed rather than the 3ENF. This is also follows for the observance of stable crack

propagation as no stable propagation occurred during 3ENF testing, and is not expected per ASTM D7905 [25].

CHAPTER 4: FINITE ELEMENT MODELING

4.1 Introduction

As of today, several failure laws have been implemented to deal with composite failure and the onset of damage, whether matrix of fiber failure. Within Abaqus, such failure criteria include Tsai-Wu, Tsai-Hill & Hashin. As for damage propagation, specifically delamination, the development of FE failure analysis has greatly increased over the past decade and now many commercial software's (Abaqus, Ansys, LS Dyna, etc.) include built-in codes for handing delamination and fracture propagation. Common numerical techniques that deal with crack propagation are Cohesive Zone Modeling (CZM) and Virtual Crack Closure Technique (VCCT). VCCT is not examined in this thesis; for background and development of VCCT, see Ronald Kruger [33]. CZM uses a traction-separation constitutive law and can deal with crack tip plasticity that may occur in ductile matrices. It is common for FEA commercial users to implement cohesive elements for CZM; another method, though fundamentally similar, is cohesive contact interaction and can be implemented in Abaqus/Standard. To the best of the author's knowledge, there is very little in the literature concerning the success of using cohesive contact for performing CZM analysis: insofar as the amount of elements needed within the process zone to accurately model coupon level testing, and model convergence. The underlying theory of cohesive elements will be presented in subsequent sections; whereas the FEA results for this thesis pertain to the use of cohesive contact interaction within Abaqus/Standard.

4.2 Literature Review

The use Cohesive Zone Modeling originated during the 1960's with Dugdale Barenblatt and has been used "as a powerful analytical tool for nonlinear fracture processes" [34]. The Barenblatt-Dugdale (BD) model introduced "the concept that stess within the zone ahead of the crack tip is limited by the materials' yield strength" [35] which creates a thin plastic zone of constant stress ahead of the crack tip. The CZ models of today do not require that the stress distribution ahead of the crack tip be constant, hence the modern "CZM is a broader generalization of the BD model" proposed decades ago [35].

CZM "relates tractions to displacement jumps at an interface where a crack may occur" [36]. The cohesive zone method models a process "ahead of the crack-tip suing traction-separation laws that relate the opening displacements in the process (or cohesive) zone to the resisting tractions. One of the simplest ways in modeling traction-separation is through the bi-linear cohesive law, as seen in Figure 24.

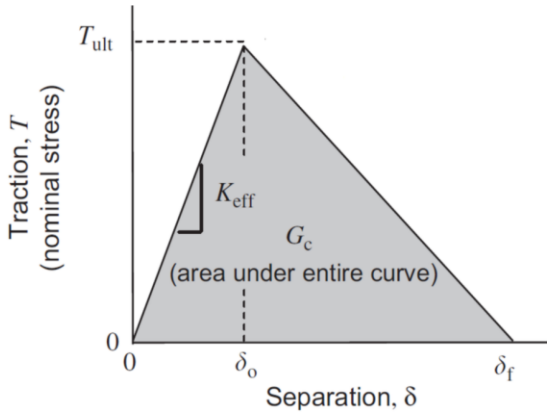

Figure 24 "Cohesive parameters of a typical bilinear traction-separation model." [37].

The bi-linear traction separation law is defined by the following parameters; initial elastic stiffness, peak traction (interfacial strength) and critical SERR which equals the area under the curve [38] as seen in the figure above.

Cohesive elements are used to model the infinitesimal cohesive layer that is presumed (per CZM) at the interface of two neighboring plies. In order to accurately predict the propagation of delamination, a "sufficiently fine finite element discretization of the cohesive zone" [38] is required to represent the tractions ahead of the crack tip. "Therefore, a minimum number of elements is needed in the cohesive zone to get successful FEM results" [36]. Additionally, a reasonable value of element stiffness must be selected to better ensure model convergence [38]; because convergence can be an issue when modeling fracture, artificial damping may be added to aid in an accurate and converged model. Numerical issues can arise because the "bi-linear law has a negative tangent stiffness in the damaged stage, requiring artificial damping to obtain a solution. This damping needs tuning by the FE analyst where excessive damping" can over-predict delamination resistance, and "too little of damping causes slow convergence" [39].

Turon et al. [40] found that cohesive zone models require very fine meshes in the cohesive zone to accurately model the tractions ahead of the crack tip. "The results indicate that a mesh size of 0.5mm or less is necessary to obtain converged solutions. The predictions made with coarser meshes significantly over predict the experimental results" [41]. Ankersen et al. [39] suggests that "a fine mesh is needed due to high stress gradients ahead of [the] cohesive zone rather than due to the cohesive zone length itself". Additionally, Yang & Cox found that "the length of the [cohesive] zone is not specified a priori, but will depend on the stress distribution near the crack tip in a particular loading

geometry" [34]. Turon [40] suggested that the interfacial strengths can be altered such that the size of the elements within the cohesive zone could be increased; leading to a model with less degrees of freedom, while still achieving model convergence.

Cohesive element theory is developed in subsequent sections, as well as cohesive surface contact which relies on the same theoretical aspects and was used for this thesis in modeling fracture testing.

4.3 Cohesive Element Theory

Abaqus allows the use of both 2D and 3D cohesive elements within its element library; including solid elements with six and eight nodes (COH3D6 & COH3D8 respectively), as well as four node elements used for 2D or axisymmetric modeling. Figure 25 illustrates the element configuration for both 2D (COH2D4) and axisymmetric (COHAX4) elements. Other than user-subroutines, such as user-defined elements, there are two ways to create 3D cohesive elements using Abaqus's element library- 1) Create (or import) a part using Abaqus CAE and mesh that part with 3D cohesive elements. 2) Offsetting elements: create a shell part with arbitrary thickness and mesh the part with shell elements. Using the element offset tool- solid or shell elements of any thickness can be offsetted from the shell part surface, in which an orphan mesh part can be created from the offsetted elements. The orphan mesh can then be re-meshed with cohesive elements and interact with other parts in the assembly module (e.g. tying the orphan mesh to top and bottom sub-laminates of a DCB test model). Once the orphan mesh is created though, it's seed size and geometry cannot be changed, in order to do so, the original shell part used for offset must be re seeded or dimensioned, followed by offsetting elements from

the most updated shell part. One of the advantages of using the element-offset method is that the element thickness can be defined as zero, such that the cohesive element material constitutive model does not need to take into account the thickness of the cohesive elements. Abaqus does not allow for the offset of elements; making zero thickness elements only possible via user-defined elements or user-material model.

If the cohesive elements and adjacent connecting parts have the same mesh seed size, than the nodes can be shared in contact amongst the cohesive and surrounding elements. If the cohesive element seed size is more or less refined than the surrounding elements, than tie constraints can be used to help ensure convergence; Figure 26 illustrates the use of tie constraints for cohesive elements with a finer mesh density than the adjacent parts.

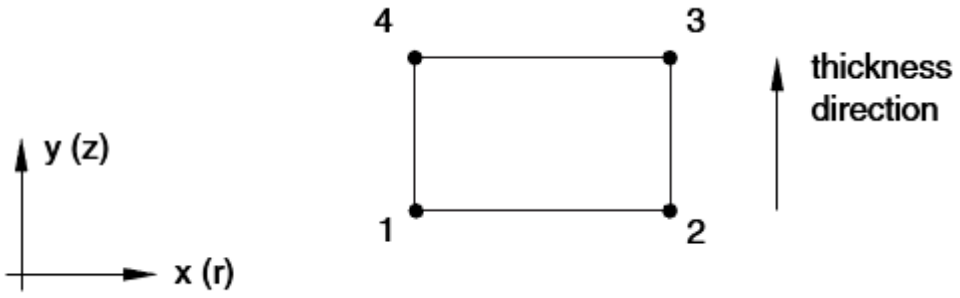

Figure 25 "Default thickness direction for two-dimensional and axisymmetric cohesive elements." [42].

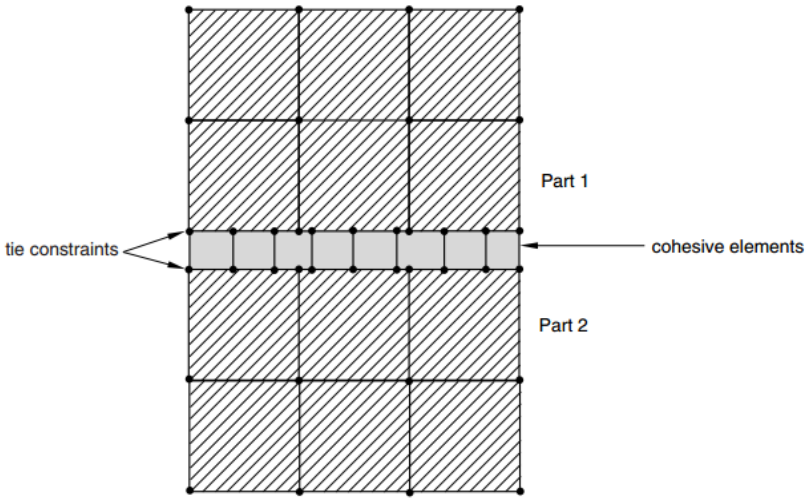

Figure 26 Part meshes with tie constraints of cohesive elements [42].

Cohesive elements are “primarily intended for bonded interfaces where the interface thickness is negligibly small” in which the constitutive response is modeled by traction-separation behavior [42]. Abaqus 6.12 Analysis User’s Manual Volume IV gives the following points considering cohesive behavior as defined by a traction-separation law [42].

- Can be used to model the delamination at interfaces in composites directly in terms of traction versus separation;
- Allows specification of material data such as the fracture energy as a function of the ratio of normal to shear deformation (mode mix) at the interface;
- Assumes linear elastic traction-separation law prior to damage;
- Assumes that failure of the elements is characterized by progressive degradation of the material stiffness, which is driven by a damage process;
- Allows multiple damage mechanisms.

4.3.1 Constitutive Response

The constitutive response for 3D cohesive elements is given in equation (38)

$$\boldsymbol{t} = \begin{Bmatrix} t_n \\ t_s \\ t_t \end{Bmatrix} = \begin{bmatrix} K_{nn} & K_{ns} & K_{nt} \\ K_{ns} & K_{ss} & K_{st} \\ K_{nt} & K_{st} & K_{tt} \end{bmatrix} \begin{Bmatrix} \delta_n \\ \delta_s \\ \delta_t \end{Bmatrix} = \boldsymbol{K\delta} \tag{27}$$

Where $\boldsymbol{t}$ is the traction vector comprised of normal traction (t_n) and shear traction components (t_s & t_t). The shear traction t_s represents the in-plane shear in the "2" direction, while t_t is the out of plane shear traction in the "3" or thickness direction. $\boldsymbol{K}$ is the stiffness of the cohesive element and has nine components for fully coupled behavior between the traction and separation vectors. Whereas $\boldsymbol{\delta}$ is the separation vector comprised of the same normal and shear components as the respective traction vector. The traction and displacement components are calculated at each integration point of the element. If the cohesive behavior is desired or expected to be uncoupled between normal and shear components, than the non-diagonal terms can be set to zero, giving equation (39)

$$\boldsymbol{t} = \begin{Bmatrix} t_n \\ t_s \\ t_t \end{Bmatrix} = \begin{bmatrix} K_{nn} & 0 & 0 \\ 0 & K_{ss} & 0 \\ 0 & 0 & K_{tt} \end{bmatrix} \begin{Bmatrix} \delta_n \\ \delta_s \\ \delta_t \end{Bmatrix} = \boldsymbol{K\delta} \tag{28}$$

For linear elastic matrices, the uncoupling assumption is reasonable; additionally, if the material is assumed to be isotropic (as in the case of a polymer matrix), than K_{nn}=K_{ss}=K_{tt}. Uncoupled behavior was assumed and used for the FEA performed in this thesis.

4.3.2 Damage Initiation

During FE simulation, a cohesive element is loaded linear elastically until a critical user-defined traction value is reached; after which the onset of damage is said to occur. This is referred to as damage initiation. Continual loading of the element post damage initiation will result in a loss of element stiffness until the element is fully degraded and will not contribute any stiffness to the model. If the loading surpasses the critical traction value, but does not achieve complete stiffness degradation, than the unloading will occur at a decreased element stiffness as seen in Figure 27.

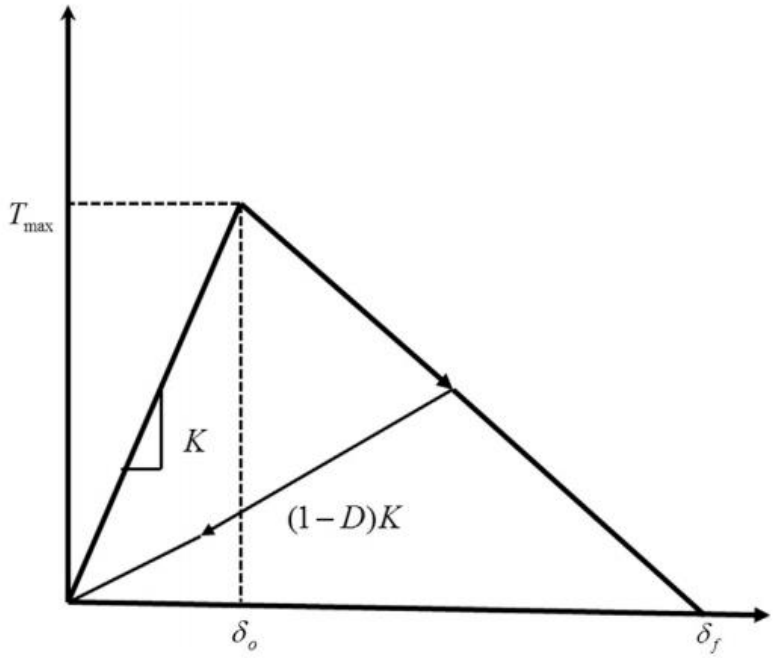

Figure 27 Bilinear traction-separation cohesive law [43].

Conversely, if the element does not reach the critical traction, than the element will still behave linearly elastically and have the same element stiffness it started with. Abaqus offers several stress and strain criteria that are used to predict damage initiation [42]; including the "maximum nominal stress criterion" and "quadratic nominal stress criterion" as presented below in equations (40) and (41) respectively

$$max\left\{\frac{\langle t_n \rangle}{t_n^o}, \frac{t_s}{t_s^o}, \frac{t_t}{t_t^o}\right\} = 1 \tag{29}$$

With the maximum nominal stress criterion, damage is assumed to initiate when any of the stress ratios in equation (40) reach unity. The ratio is defined to be the current stress divided by the critical stress (or traction), as inputted by the user. The Macaulay brackets

encompassing the normal stress component “are used to signify that a pure compressive deformation or stress state does not initiate damage.” [42].

$$\left\{\frac{\langle t_n \rangle}{t_n^o}\right\}^2 + \left\{\frac{t_s}{t_s^o}\right\}^2 + \left\{\frac{t_t}{t_t^o}\right\}^2 = 1 \tag{30}$$

The quadratic nominal stress criterion assumes that damage initiates when the square of the before mentioned stress ratios reach unity. If mixed mode loading occurs, then damage initiates if the sum of the quadratic normal and shear stress ratios reach a value of one.

4.3.3 Damage Evolution

Damage evolution describes how “the rate at which the material stiffness is degraded once the corresponding initiation criterion is reached.” [42]. The manner in which the material stiffness degrades is dependent on which evolution law is used: the simplest damage evolution law has linear softening after damage initiation occur. The term softening expresses how the element stiffness decreases once damage is initiated. Abaqus also offers an exponential softening law and can be found in [42].

The complete bilinear traction-separation cohesive law (Figure 27) contains the linear elastic loading until damage onset is reached, followed by the linear softening rule as the element stiffness is degraded until max displacement is achieved, and the element is fully degraded. The element stiffness K, in the elastic region, is defined as

$$K_i = \frac{t_i}{\delta_i^o} \tag{31}$$

Where i=1,2,3 so that equation (42) can be used for all three traction & displacement components respectively. The term $\delta_i^o$is the displacement at which damage initiation occurs; hence equation (42) is only valid up to the onset of damage. If isotropic behavior is assumed, then K_{nn}=K_{ss}=K_{tt}. The scalar value D is the damage variable which determines how much the element stiffness has degraded during damage evolution, and ranges from 0 to 1 depending on how far loading has occurred past damage initiation. In terms of the original element stiffness, and the damage variable, the degraded element stiffness is defined to be

$$\bar{K} = (1 - D)K \tag{32}$$

One method in defining the damage evolution is to base the damage process on the fracture energy of the interface. The fracture energy is determined a priori from mechanical testing and is inherently the only "real life" parameter used in cohesive modeling. The normal and shear tractions & displacements do have tangibility w.r.t relating an FE model to reality, but actually vary on element seed size and can be calibrated to successfully match the model to empirical testing; therefore they are not mechanical properties such as fracture energy. From Figure 27, the fracture energy is defined as

$$G_C = \frac{T_{max}\delta_o}{2} \tag{33}$$

For a pure mode I case, the energy based damage evolution criterion is

$$\left\{\frac{G_I}{G_{IC}}\right\} = 1 \tag{34}$$

When the energy of the element reaches that of the critical fracture energy, the element will be completely degraded and no longer contribute stiffness to the model. In general, for 3D cases, the energy based evolution criterion is given by

$$\left\{\frac{G_I}{G_{IC}}\right\}^{\alpha} + \left\{\frac{G_{II}}{G_{IIC}}\right\}^{\beta} + \left\{\frac{G_{III}}{G_{IIIC}}\right\}^{\gamma} = 1 \tag{35}$$

Such that if mixed mode loading occurs, the element will reach full degradation is the sum of respective normal and shear fracture energy ratios equals unity. Exponents α, β and γ can be found thru testing but can be difficult to do so considering full 3D mixed mode behavior is still not fully understood. The two most common assumptions when using equation (46) are 1) Linear law: α=β=γ=1 and 2) Power law: α=β=γ=2. See [42] for more energy based damage evolution criteria and cohesive element theory in general. For this thesis, 1D damage evolution was performed [equation (45)] since only DCB (mode I) specimens were modeled.

4.3.4 Cohesive Parameters

The element stiffness K is a penalty parameter that must be carefully chosen in order to ensure model convergence; if K is too low or too high, numerical instability will occur and convergence is highly unexpected. Additionally, the penalty stiffness must be large enough "to prevent interpenetration of the crack faces and to prevent artificial compliance that can lead to numerical problems." [38]. Turon, et al. [36] proposed the following equation for choosing the element penalty stiffness

$$K \geq \frac{\alpha E_3}{t} \tag{36}$$

Where E_3 is the modulus of elasticity in the thickness direction; which, for uni-directional laminates, is equal to the transverse modulus E_2. This assumption can be made due to the transversely isotropic material classification of uni-directional layups. The variable t is the thickness of an adjacent sub-laminate: Turon suggested that α=50 for calculating a reasonable stiffness of the cohesive interface that can produce converged results.

As alluded to previously in section 2.9 a small process zone occurs ahead of the crack tip during fracture. This process zone (a.k.a. cohesive zone) relates the crack tip opening displacements to the tractions developed near the crack tip that resist crack propagation. "For typical graphite-epoxy materials, the length of the cohesive zone is less than 1 mm." [38]. In order to accurately represent "the distribution of tractions ahead of the crack-tip" [38], a sufficient amount of elements must be present within the cohesive zone. Mathematically, the cohesive zone length for mode I fracture is defined by equation (48) below.

$$l_{cz\_I} = \frac{\mathrm{E}_2 G_{IC}}{t_n^2} \tag{37}$$

The length of the cohesive element is given as

$$l_e \leq \frac{l_{cz\_}I}{N_e} \tag{38}$$

Where N_e is the amount of elements desired to be within the cohesive zone. Once the user calculates, or picks a cohesive zone length, they decide how many elements will be within the process zone and use equation (49) to calculate the element length.

If the normal traction is not known, or previous values are not leading to convergence, then equation (50) can be used to calculate the normal traction necessary to ensure equilibrium, provided remaining parameters have been chosen (N_e), calculated (l_e) or determined experimentally (E_2 & G_{IC}).

$$t_n = \sqrt{\frac{E_2 G_{IC}}{N_e l_e}} \tag{39}$$

For modeling mode I fracture, the following parameters must be user-defined within Abaqus: K_{nn}, t_n, and G_{IC}. For determining the required mesh size; the number of elements within the cohesive zone is decided by the user, followed by using equation (48).

4.4 Cohesive Contact

In addition to cohesive elements, Abaqus allows the use of cohesive surface contact to model delamination and cohesive interfaces. The underlying theory used for cohesive elements is the same as cohesive contact such as; traction-separation constitutive relation, bilinear traction law, damage initiation & evolution, penalty stiffness and elements within the process zone. The major difference is that Instead of creating a separate part (conventionally or as an orphan mesh part), the cohesive contact behavior is assigned to the master and slave surfaces respectively. Just like regular contact assignment within Abaqus, it is recommended that the slave surface have a finer mesh than the master surface. Since the DCB specimen is a balanced and symmetric laminate, it is arbitrary as to which sub-laminate is chosen to be the master or slave surface.

4.4.1 Implementation of Cohesive Contact Interaction within Abaqus/Standard

The following is a detailed layout of how to implement cohesive surface contact within Abaqus/Standard. The example given relates to the work performed in this thesis.

- Part Module: Create new part (2D deformable shell)

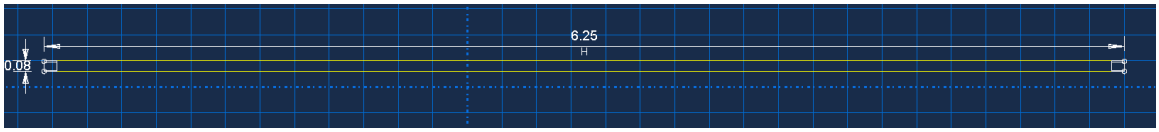

- This part is one sub-laminate; copy this part for the second sub-laminate
- Partition the edges on the mid plane edge of each respective sub-laminate.

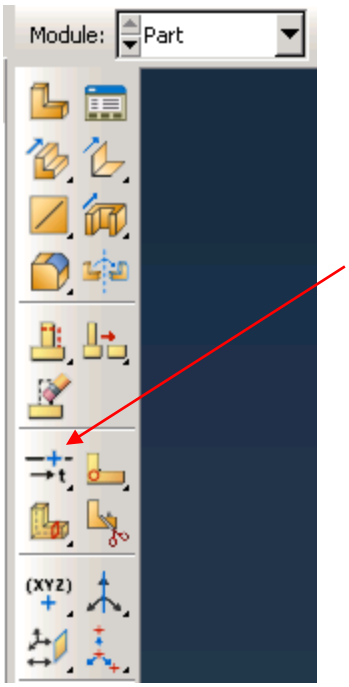

- Select the edges interface edges “individually”; top and bottom sub-laminate respectively

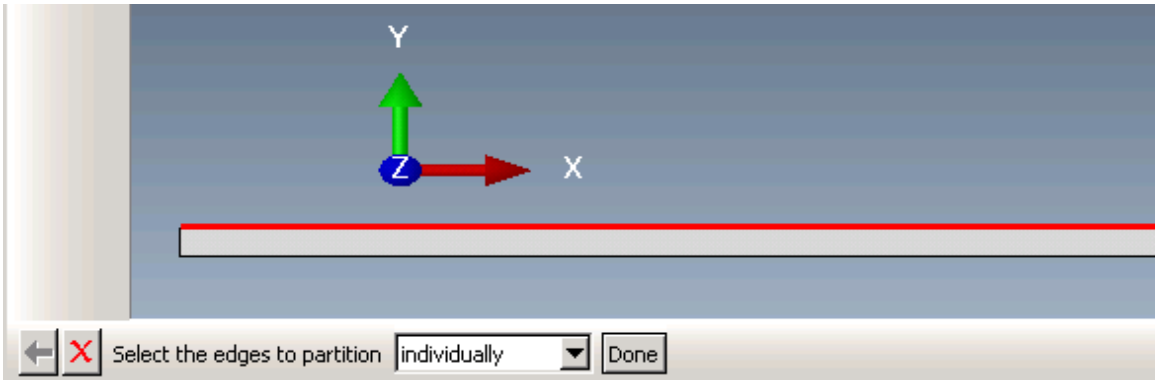

- The normalized edge parameter is normalized by the edge length; entering “.5” will partition the edge halfway along the edge, whereas entering “.75” will partition the edge 75% along the length as defined by the partition direction

- A edge parameter value of “.32” corresponds to a 2” delamination length (per ASTM D5528) for a 6.25” long DCB specimen.

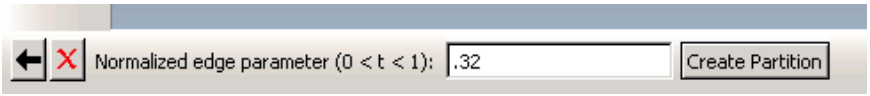

- Property Module: Enter Elastic material properties; use type “Engineering Constants”

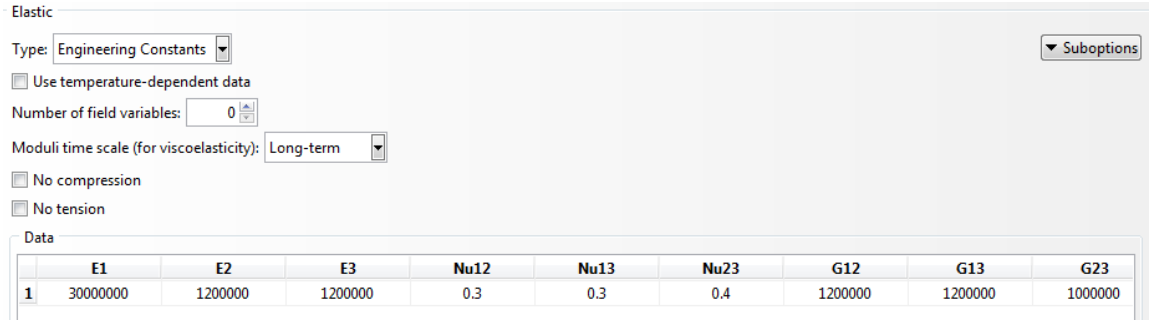

- Apply “Solid Homogenous” section to both sub-laminates
- Assembly Module: Create an instance for each sub-laminate
- Step Module: Create “Static, General” step

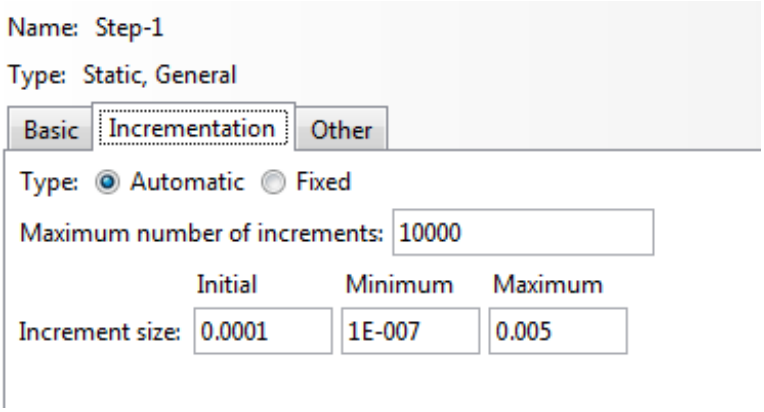

- Convergence is of concern for CZM; relatively small increments should be used as well as providing a maximum number of increments if convergence becomes an issue.
- Click on “Other” tab while in Step Module

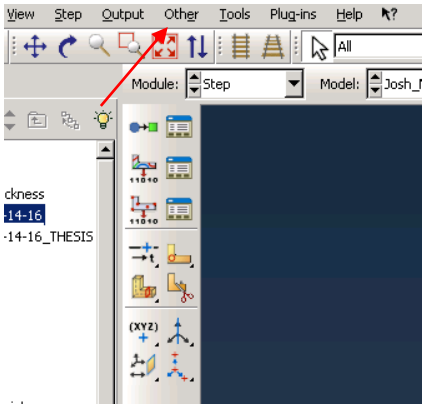

- [General Solution Controls => Edit => "Analysis Step name"]
- The following Warning will pop up; press continue

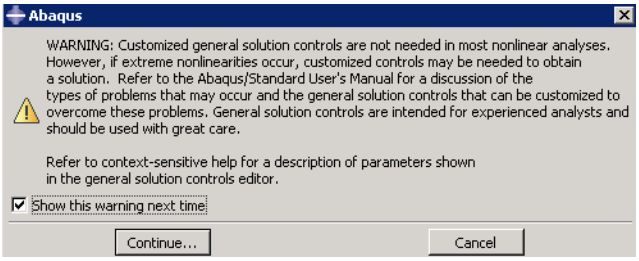

- Select "Discontinuous analysis"

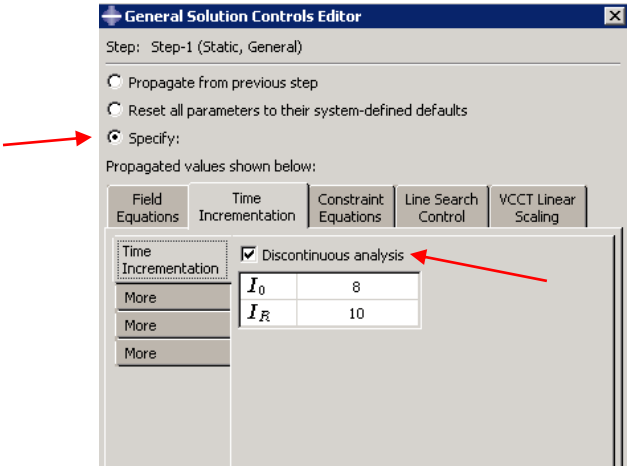

- Select “More” on left menu, increase “I_A” considerably, say 30. I_A represents the amount of failed convergence attempts Abaqus will allow before the job is aborted. More attempts may be required for non-linear FEA such as fracture.

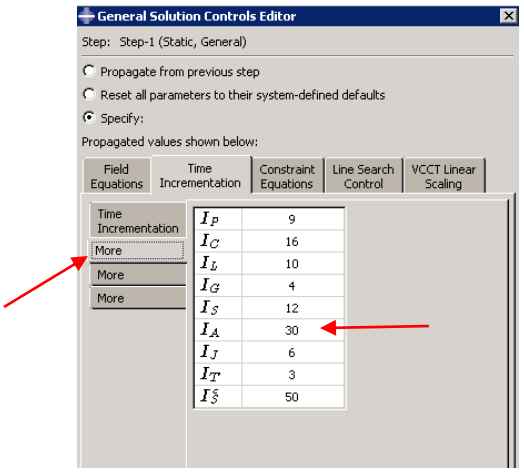

- Interaction Module: Use “Interaction Property Manager” to create cohesive contact interaction property. Select “Damage” & “Cohesive Behavior” from Mechanical tab.
- Assign cohesive stiffness values.

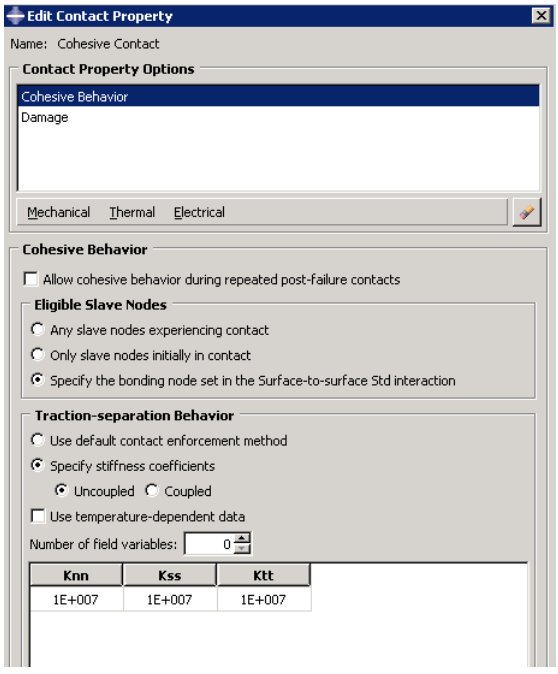

- Assign Damage Initiation; select desired criterion.

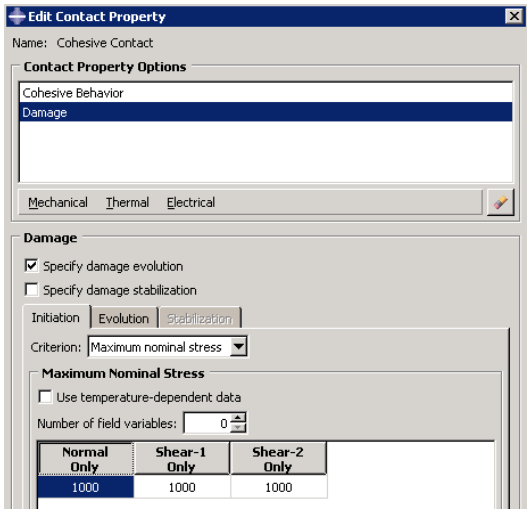

- Assign Damage Evolution; select Energy and Linear for type & softening respectively.

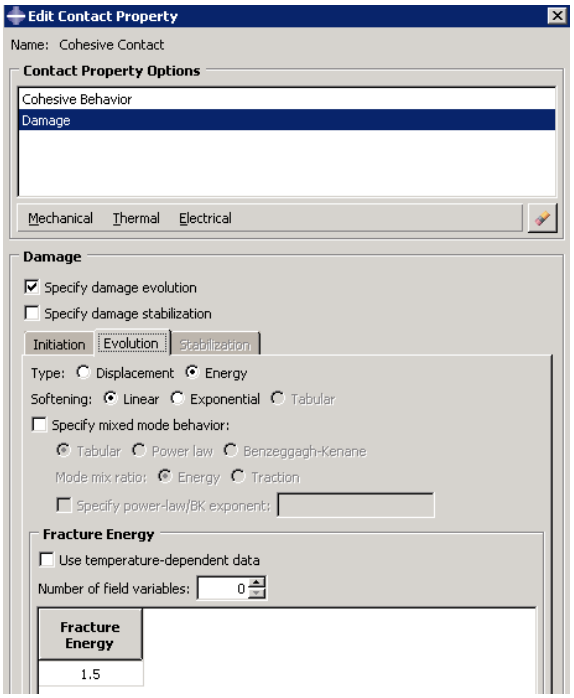

- Using Interaction Manager, create an Interaction for which the Cohesive Contact property is assigned.

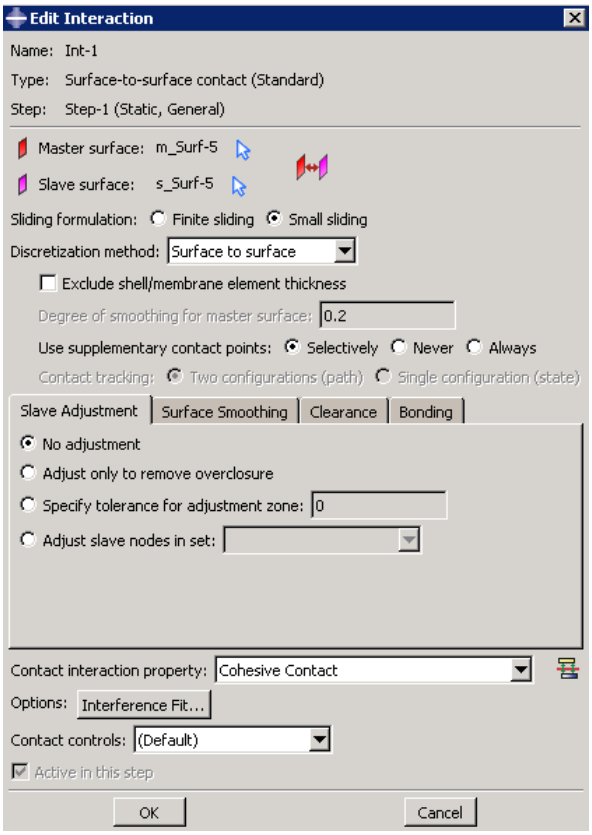

- Select Master and Slave surfaces.

- Assembly Module: Translate the sub-laminates such that they are in proper contact with one-another. “Coincident point” in the Constraint tab may be used, as seen below

- Load Module: Apply boundary conditions to the face of each sub-laminate

- Where $\delta/2$ is half of the opening displacement observed in DCB testing.
- Mesh Module: seed part as desired. For this thesis, the vertical edges of each sub-laminate were seeded by edge with eight elements per edge.
- Seed horizontal edges with desired size. Three elements are within cohesive zone of top sub-laminate, whereas two elements are within cohesive for bottom sub-laminate. Cohesive zone was chosen as 1mm (.039in).

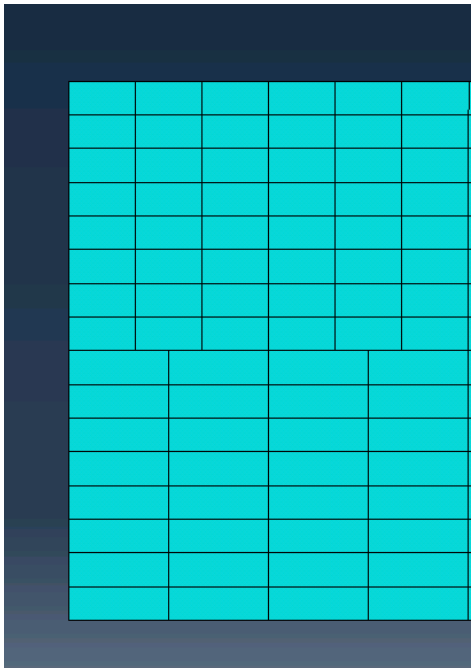

- Create a node set on loaded face(s) of beam. Either (or both) sub-laminates may be chosen.

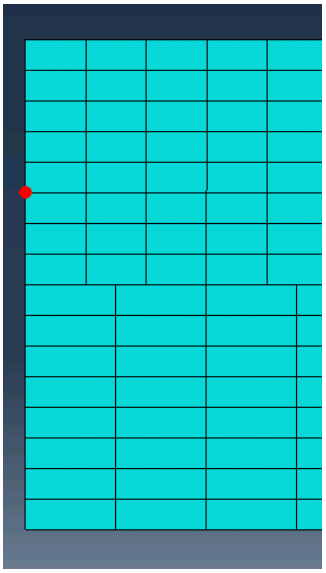

- Return to Step Module: Edit History Output- “History Output Manager”.
- Change “domain” to “Set”, and select the node set previously created.
- Select “$U2$” & “$RF2$” for Output Variables.

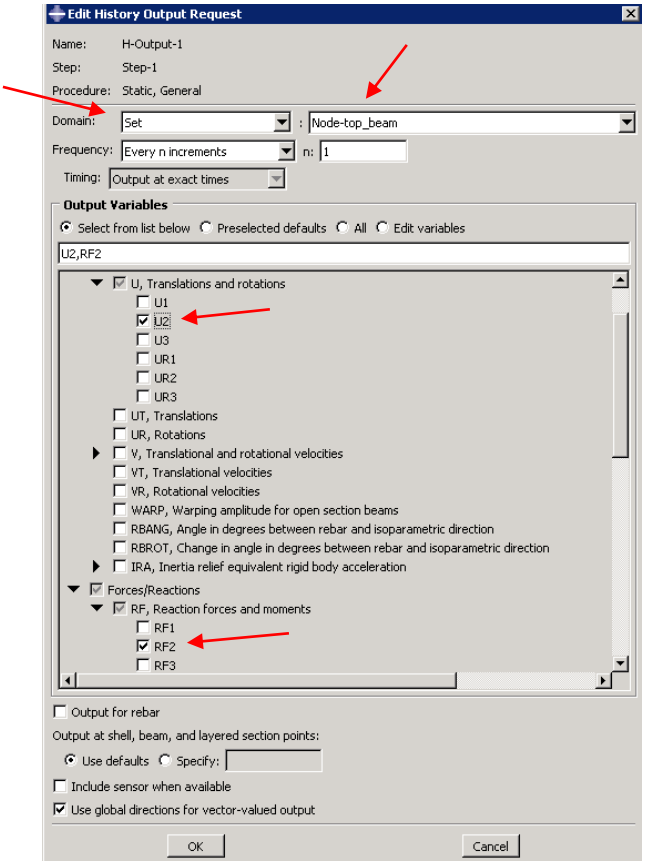

- Job Module: Create and run Job.
- Display Results and create an XYData plot from Output History

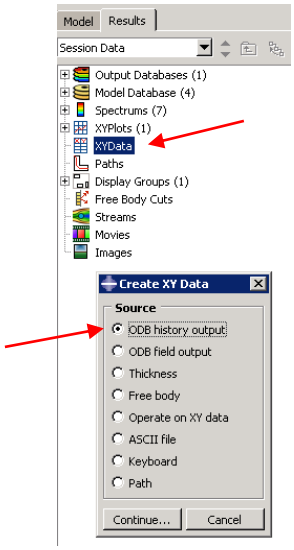

- Select "*RF*2" as Output History plot variable

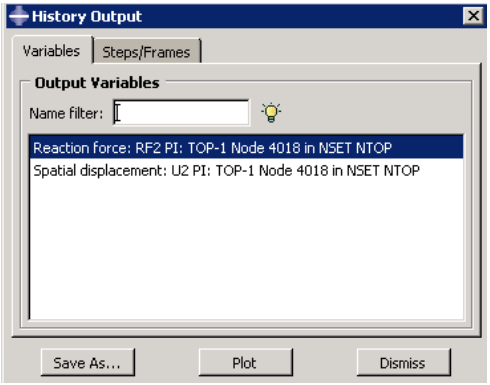

- Plot values can be exported into Microsoft Excel/etc.

4.5 Results

4.5.1 FE Calibration of DCB Experiment

Before fracture testing was performed, an FE model was created to simulate the DCB testing performed by Josh Smith [1]. Unlike the work presented in this thesis, Josh Smith tested cloth composite specimens for DCB fracture testing.

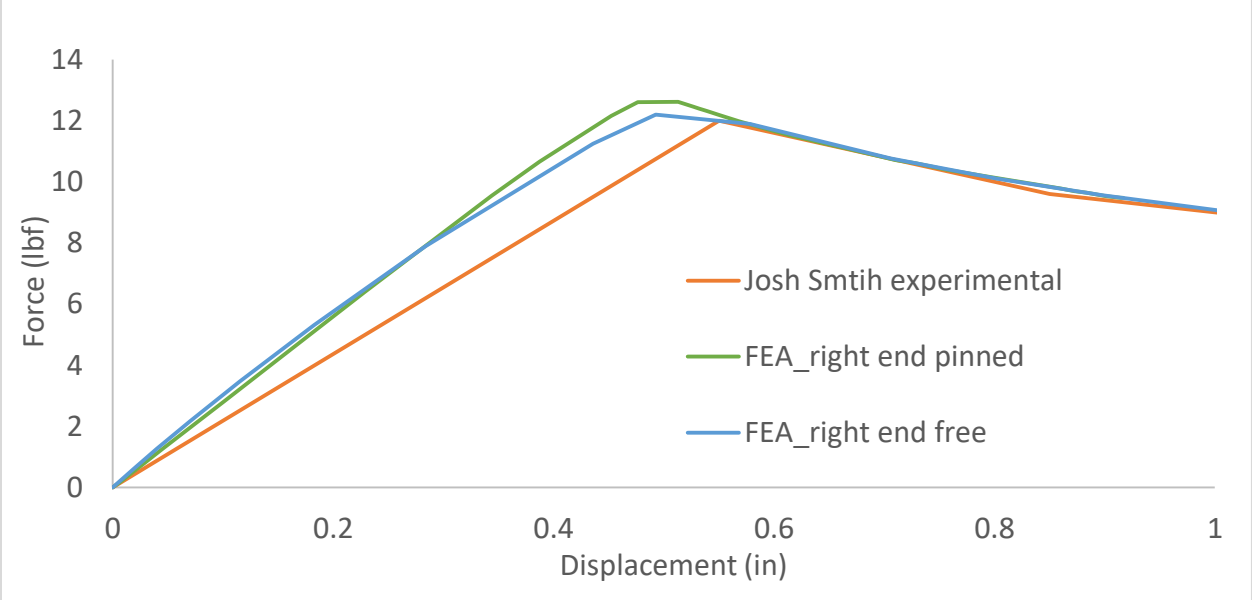

Figure 28 DCB P-δ curve; FEA calibration of J. Smith data [1].

The first FE model had the right end pinned, with the displacement boundary conditions applied to the left side faces of each sub-laminate. As seen in Figure 28, pinning the right end overestimated P_{max} and the beam stiffness as compared to leaving the right end free with no b.c's. The second model removed the b.c's on the right end

which slightly increased the accuracy of the P-δ prediction compared to the initial, more restricted model. This result was expected as pinning the right end adds restriction to the DCB opening up, which artificially increases the stiffness of the beam. Steady state fracture matched that of the experimental data in both models though, despite having different P_{max} loads, and where they occurred in terms of opening displacement.

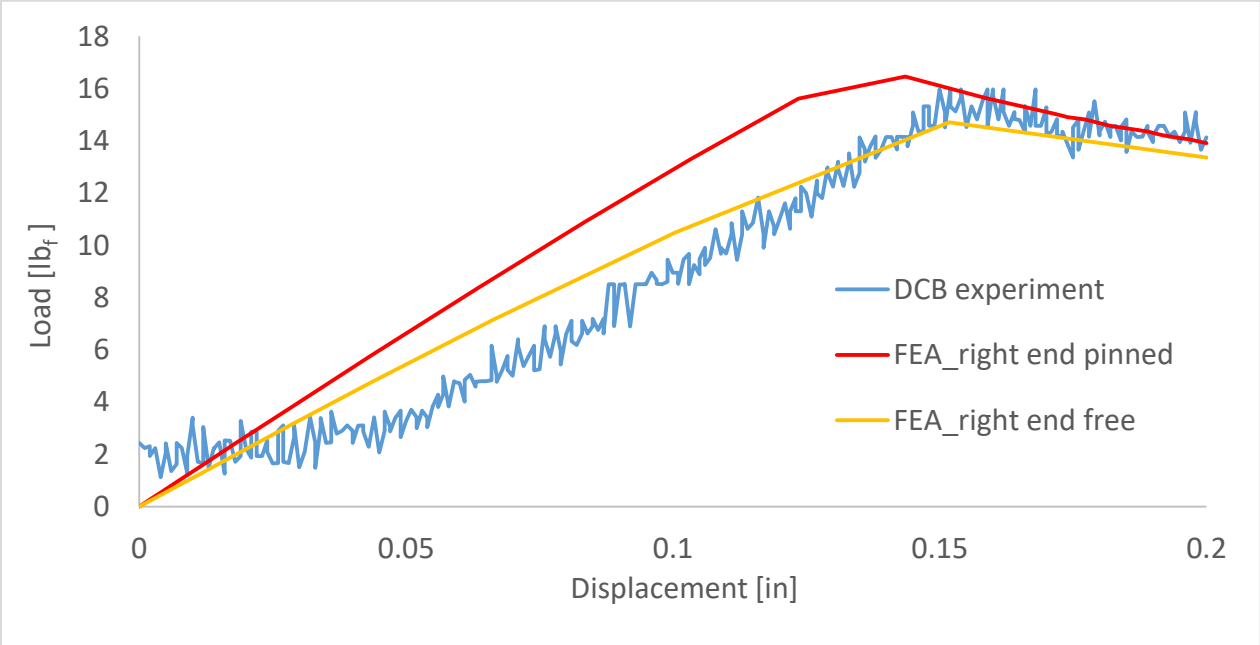

Figure 29 DCB P-δ curve; FEA calibration of mode I data.

Of the three DCB specimens tested, the P-δ curve of specimen TE-S2 was selected for FE calibration. As seen Figure 29, pinning the right end of the DCB significantly increased the stiffness of the beam, whereas freeing the right end b.c produced a P-δ curve having good agreement with the experimental data. Comparing Figure 28 & Figure 29, the discrepancy in stiffness between pinning and not pinning the right end of the DCB is quite noticeable. The best explanation for this discrepancy

difference relates to the variance in Modulus values for both cloth & uni-directional laminates. For cloth, E_1=E_2 and will be significantly lower than E_1 of the uni-directional counterpart, resulting in a larger beam stiffness discrepancy when applying pinned b.c's to the non-loading end. The converged model parameters for TE-S2 are below in Table 6; Table 7 for used material properties.

Table 6 Cohesive contact parameters for converged FE model.

K (lb/in)	T (psi)	G (Psi-in)	Ne
$10x10^6$	1000	1.5	3

Table 7 M46J/TC250 material properties used for cohesive contact FE model.

E_1 (Msi)	E_2, E_3 (Msi)	ν_{12}, ν_{13}	ν_{23}	G_{12}, G_{13} (Msi)	G_{23} (Msi)
30	1.2	.3	.4	1.2	1

With equation (47), the cohesive stiffness was calculated to be over $80x10^7$ lb/in- causing numerical instability and a lack of model convergence. Lowering the stiffness to $10x10^7$ lb/in allotted for better results, but caused instability near the peak load and aborted the job in Abaqus before reaching steady state fracture. A stiffness of $10x10^6$ lb/in was found to ensure convergence. The cohesive zone was assumed to be 1mm (0.039 in) per [38], N_e was chosen to be 3, such that l_e was 0.013 in. Using equation (50), the critical traction was calculated to be 2148 psi. The model converged with this traction value, but the beam stiffness and peak load overestimated the empirical data. The traction was chosen as 1000 psi and best matched the DCB test data.

4.5.2 Parametric Study

A parametric study of four cohesive parameters was performed: normal traction (t_n), cohesive stiffness (K), fracture energy (G_{IC}), and elements within the cohesive zone (N_e). The range chosen for the parametric study was 80%-120% of the cohesive parameters of the converged model. Varying the traction and stiffness within this range did not alter the results; these results can be found in Appendix B The results of varying G_{IC} and l_e are seen below in Figure 30 and Figure 31.

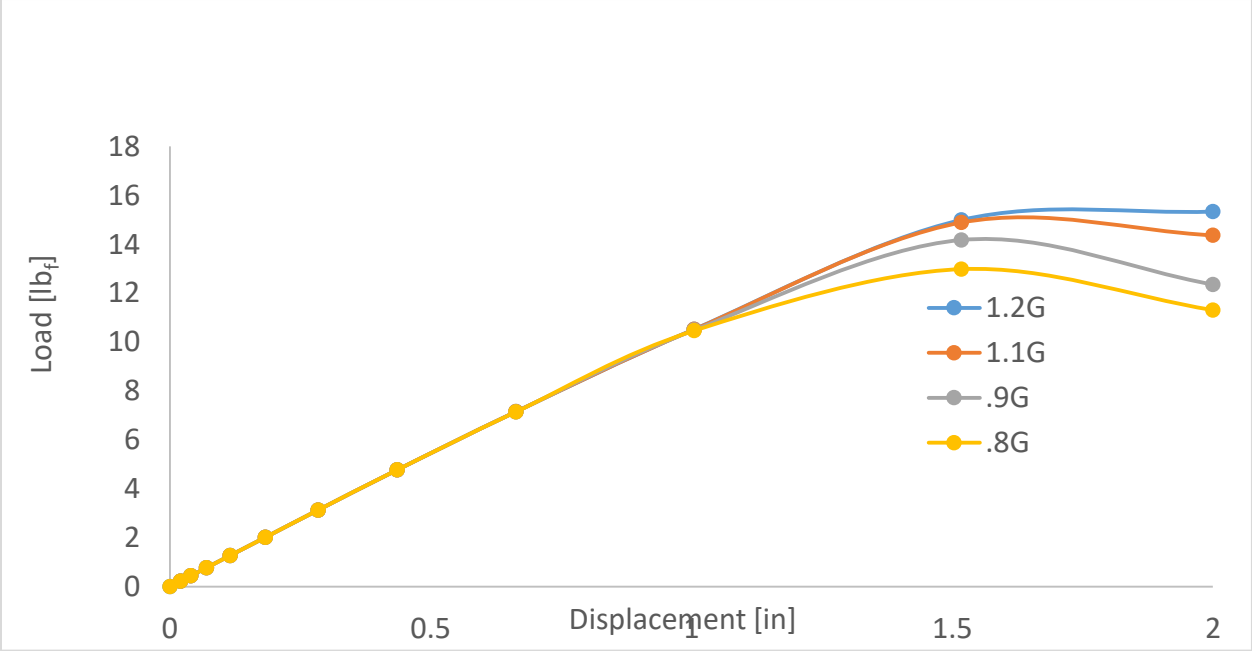

Figure 30 DCB P-δ curve for 80%-120% range of experimentally determined mode I fracture energy.

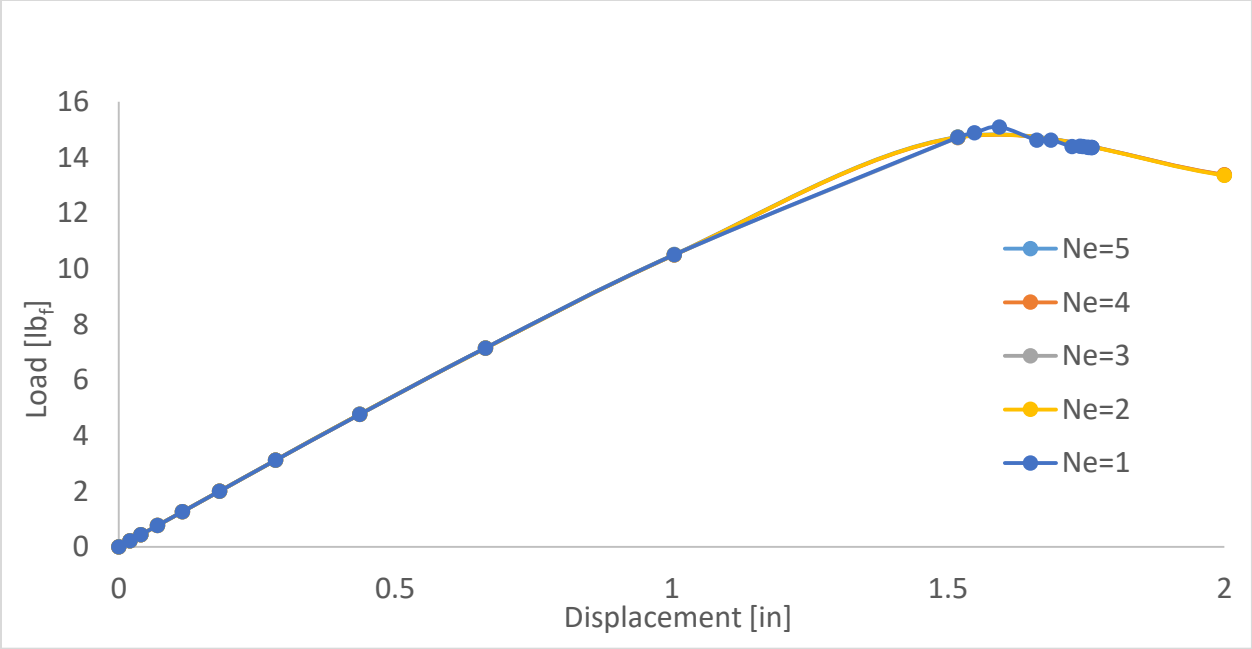

Figure 31 Range of elements within laminate process zone ahead of crack tip.

Changing the fracture energy altered the P-δ curve; this was to be expected as the fracture energy is determined a priori and represents the interfaces ability in resisting damage, hence increasing the strength of the interface will increase the max load reached during DCB loading. Seeing that the P-δ did not vary by having N_e range from 1-5 was not to be expected. The literature for cohesive elements suggests that 3-5 elements should be used within the cohesive zone, to the best of the author's knowledge, no such recommendation has been found for when using cohesive contact. The slight discrepancy in Figure 31 regarding N_e=2 has to do with contact algorithms in Abaqus and is not a reflection of cohesive behavior. When performing contact analysis, the master and slave surfaces should not have the same seed size (if possible). The results in Figure 31 are relative to the slave surface which should be meshed finer than the master surface. For

N_e=2, the master and slave surface had the same mesh refinement, hence the slight variance in the P-δ curve.

Seeing that the load-displacement curve did not change for when N_e=1 can give some insight into the usefulness of cohesive contact as a potential substitute for cohesive elements for simple DCB modeling. The literature recommends not only that 3-5 cohesive element be within the cohesive zone, but that the length of the cohesive elements within the zone be no greater than 0.5mm (0.0195in). The cohesive contact model was not sensitive to varying N_e from 1-5 elements within the process zone. This is key considering as the length of the elements within the cohesive zone decrease, the size of the model (d.o.f's) rapidly increases and will increase the time needed to obtain a solution. The cohesive contact FE model ran efficiently as the step increment size did not drop below 0.001 and the model converged within minutes giving no errors or warnings. Additionally, viscous damping (damage stabilization) was not needed as the model did not encounter numerical difficulties in obtaining convergence. Considering the convergence time, lack of damping, insensitivity to element length, and an overall ease in building and implementing the FE model, the use of cohesive surface contact in Abaqus/Standard can be advantageous for DCB simulation as compared to using cohesive elements. Further study of cohesive contact is recommended, particularly for other modes of failure, considering there is presently very little (if any) within the literature in using cohesive surface contact.

CHAPTER 5: CONCLUSIONS

DCB, ENF and 4ENF specimens were tested to characterize the mode I & mode II fracture energy of 18 ply uni-directional laminates made of M46J/TC250. Testing standards ASTM D5528 & ASTM D7905 were used (where deemed relevant) for obtaining mode I and mode II fracture energies. 4ENF specimens were also tested to inquire the validity of the 4ENF test as compared to the ENF. Two built-in delamination methods were used; mold release application and use of a PTFE insert. A finite element model using cohesive contact interaction within Abaqus/Standard was performed to simulate mechanical fracture testing of DCB specimens. Additionally, a parametric study of cohesive parameters was performed to investigate the sensitivity of the main Abaqus parameters used for CZM per cohesive surface contact. From the research and work performed, the following conclusions can be made:

- Non pre-cracked and pre-cracked DCB specimens exhibited similar steady state fracture behavior.
- The PTFE insert method was found to provide a more reliable built-in delamination than using the mold release. The potential effectiveness of the mold release as a built-in delamination method is inconclusive though, as a lower quality release was used and better results are assumed with a higher quality mold release.
- Fiber-bridging significantly increased the fracture resistance of DCB specimens. The occurrence of fiber-bridging was unique to each built-in delamination method- one or two large ligaments bridged between top & bottom sub-laminates

for mold release specimens, whereas several individual fibers bridged across the sub-laminates for specimens with a PTFE insert.

- 4ENF was observed to be a more suitable test for G_{IIC} than the ENF fixture per ASTM D7905. 4ENF exhibited stable crack propagation, whereas no stable crack propagation occurred for the ENF specimens. 4ENF is equally as simple to set up and perform as ENF, and is approximately 10-12 times quicker to perform than ENF as compliance calibration is not required, nor the recording of the crack length during displacement loading. 4ENF specimens with PTFE inserts yielded similar G_{IIC} values as those with mold release delaminations.
- FEA cohesive modeling is iterative; fracture energy must be obtained (or assumed) a priori.
- Surface traction and stiffness values are not physically tangible and can be adjusted through a sufficiently wide range in order to fine tune the FE model for accurate simulations.
- Using cohesive contact interaction for 2D simulations is efficient and simpler to implement than 2D cohesive elements. Likewise, to the knowledge of the author, the number of elements within the process zone is less of a concern with cohesive contact than with the use of cohesive elements; having 1-5 elements within the process zone negligibly altered the results for cohesive contact interaction. Cohesive elements however, per the current literature, should be implemented such that at least 3 elements are within the fracture process zone ahead of the crack tip.

- Coupon level testing can be successfully modeled with the use of FE software, but more complicated tests should be performed to validate real world structures in which the fracture mode interactions are more complicated. Sub-modeling of large structures is recommended.

BIBLIOGRAPHY

[1] J. Smith, "Mode I Fracture of Eight-Harness-Satin Carbon Cloth Weaves for Co-Cured and Post-Bonded Laminates," San Luis Obispo, 2014.

[2] O. A. Bauchau, "Material property definition," [Online]. Available: http://www.dymoresolutions.com/dymore4_0/UsersManual/StructuralProperties/MatProp.html.

[3] [Online]. Available: https://www.google.com/patents/US20140272324.

[4] Delaware Composites Design Encyclopedia, Failure Analysis of Composite Materials, vol. 4, Technomic Publishing company, 1990.

[5] K. P. C. R. E.E Gdoutos, Failure Analysis of Industrial Composite Materials, McGraw-Hill, 2000.

[6] L. J. B. K. C. Bhagwan D. Agarwal, Analysis and Performance of Fiber Composites, John Wiley & Sons , 2006.

[7] W. Ding, "Delamination Analysis of Composite Laminates," Toronto, 1999.

[8] Elsevier Science Ltd. , Fracture of Polymers, Composites and Adhesives, vol. 27, A. P. j.G. Williams, Ed., ESIS Publication, 2000.

[9] F. Paris, "A Study of Failure Criteria of Fibrous Composite Materials," Langley Research Center, Hampton, Virginia, 2001.

[10] J. Z. R. W. Michael Janssen, Fracture Mechanics, 2, Ed., Spon Press, 2002.

[11] P. Rusmee, "Fracture Failure of Engineering Materials," 1998. [Online]. Available: http://www.mech.utah.edu/~rusmeeha/labNotes/fracture1.html.

[12] [Online]. Available: https://en.wikipedia.org/wiki/Fracture.

[13] Impact solutions, [Online]. Available: http://www.impact-solutions.co.uk/fracture-toughness-determination-iso-17281-now-available/.

[14] D. D. Adams, "Mixed-mode fracture toughness of composites," Composites World, 2009.

[15] B. B. P. A.J. Brunner, "A status report on delamination resistance testing of polymer-matrix composites," Elsevier Ltd, 2008.

[16] G. S. B. B. P. Davies, "Comparision of Test Configurations for the Determination of GIIC: Results from an Internation Round Robin," *Plastics, Rubber and Composites*, vol. 28, no. 9, 1999.

[17] J. &. J. R. R. John H. Crews, "A Mixed-Mode Bending Apparatus For Delamination Testing," NASA, 1988.

[18] A. Szekrenyes, "Delamination fracture analysis in the GII-GIII plane using prestressed transparent composite beams," Elsevier, Budapest, Hungary, 2006.

[19] J. G. Ratcliffe, "Characterization of the Edge Crack Torsion (ECT) Test for Mode III Fracture Toughness Measurement of Laminated Composites," National Research Council, Hampton, Virginia .

[20] A. B. S. A. M.R.M. Aliha, "Determination of mode III fracture toughness for different materials using a new designed test configuration," Elsevier , 2015.

[21] D. Z. Youjiang Wang, "FEM and Experimental Analysis of Mode III Fracture Behavior of Composite Laminates".

[22] J. V. A. A. S. R. V. M. A Lopez-Menedez, "A new method for testing composite materials under mode III fracture," Journal of Composite Materials, 2016.

[23] D. D. A. Adams, "Compact tension fracture toughness testing," Composites World, 1 July 2014. [Online]. Available: http://www.compositesworld.com/articles/compact-tension-fracture-toughness-testing.

[24] American Society for Testing and Materials, "Standard Test Method for Mode I Interlaminar Fracture Toughness of Unidirectional Fiber-Reinforced Polymer Matrix Composites," ASTM International, 2013.

[25] American Society for Testing and Materials, "Standard Test Method for Determination of the Mode II Interlaminar Fracture Toughness of Uniderectional Fiber-Reinforced Polymer Matrix Composites," ASTM International, 2014.

[26] M. F. S. F. d. Moura, "Interlaminar Mode II Fracture Characterization," Porto.

[27] "Shear and moment diagram," [Online]. Available: https://en.wikipedia.org/wiki/Shear_and_moment_diagram.

[28] B. D. D. Clara Schuecker, "Evaluation of the accuracy of the four-point bend end-notched flexure test for mode II delamination toughness determination," ELSEVIER, Syracuse, NY, 2000.

[29] T. C. V. Alfred Franklin, "Generation of R-Curve from 4ENF Specimens: An Experimental

Study.," Hindawi Publishing Corporation, 2014.

[30] M. N. Y. T. T. M. Wen-Xue Wang, "Experimental investigation on test methods for mode II interlaminar fracture testing of carbon fiber reinforced composites," ELSEVIER, 2009.

[31] F. P. A. P. Giuseppe Marannano, "Numerical and experimental analysis of the frictional effects on 4ENF delamination tests performed on unidirectional CFRP," ELSEVIER, 2015.

[32] P.-Y. B. J. J.-J. R. C. Chengye Fan, "Internal-Notched Flexure Test for Measurement of Mode II Delamination Resistance of Fibre-Reinforced Polymers," Hindawi Publishing Corporation, 2013.

[33] R. Kruger, "Virtual crack closure technique: History, approach, and applications," American Society of Mechanical Engineers, Hampton, VA, 2004.

[34] B. C. Qingda Yang, "Cohesive models for damage evolution in laminated composites," Springer, Thousand Oaks, CA, 2005.

[35] A. M. W. De Xie, "Discrete cohesive zone model for mixed-mode fracture using finite element analysis," ELSEVIER, Ann Arbor, MI, 2006.

[36] A. T. TRAVESA, "SIMULATION OF DELAMINATION IN COMPOSITES UNDER QUASI-STATIC AND FATIGUE LOADING USING COHESIVE ZONE MODELS," 2007.

[37] R. E.-H. Donna Chen, "Cohesive Fracture Study of a Bonded Coarse Silica Sand Aggregate Bond Interface Subjected to Mixed-Mode Bending Conditions," Calgary, Alberta Canada, 2013.

[38] K. Song, "Guidelines and Parameter Selection for the Simulation of Progressive Delamination," NASA Langley Research Center, Hampton, VA, 2008.

[39] G. D. J. Ankersen, "Interface elements- advantages and limitations in CFRP delamination modeling," London, UK.

[40] J. C. P. P. C. P. M. Albert Turon, *Analytical and Numerical Investigation of the Length of the Coheisve Zone in Delaminated Composite Materials,* Girona, Spain.

[41] C. D. P. C. J. C. A. Turon, "An engineering solution for mesh size effects in the simulation of delamination using cohesive zone models," ELSEVIER, Porto, Portugal, 2006.

[42] D. Systems, "Abaqus Analysis User's Manual Volume IV," 2012.

[43] P. G. A. R. I. R. R. D. M. A. J. K. Mei Qiang Chandler, "Finite element modeling of multilayered structures of fish scales," Elsevier, 2014.

[44] G. Rodriguez, FINITE ELEMENT MODELING OF DELAMINATION DAMGE IN CARBON FIBER LAMINATES SUBJECT TO LOW-VELOCITY IMPACT AND COMPARISION WITH EXPERIMENTAL IMPACT TESTS USING NONDESTRUCTIVE VIBROTHERMOGRPAHY EVALUATION, San Luis Obispo, CA: George Rodriguez, 2016.

[45] T. Abbey, "FEA and Composites, Part 1," 1 October 2014. [Online]. Available: http://www.deskeng.com/de/fea-composites-part-1/.

[46] R. M. Jones, Mechanics of Composite Materials, Hemisphere Publishing Corporation, 1975.

[47] [Online]. Available: http://www.ltas-cm3.ulg.ac.be/FractureMechanics/img/Picture50_overview.png.

[48] R. M. Christensen, "2013 Timoshenko Medal Award Paper- Completion and Closure on Failure Criteria for Uniderectional Fiber Composite Materials," Stanford, 2013.

[49] A. S. f. T. a. Materials, "Standard Test Method for Determination of the Mode II Interlaminar Fracture Toughness of Uniderectional Fiber-Reinforced Polymer Matrix Composites," ASTM International, 2014.

[50] "Composite Materials," [Online]. Available: http://www.efunda.com/formulae/solid_mechanics/composites/calc_ufrp_cs_arbitrary.cfm.

APPENDICES

Appendix A. Cure Cycle

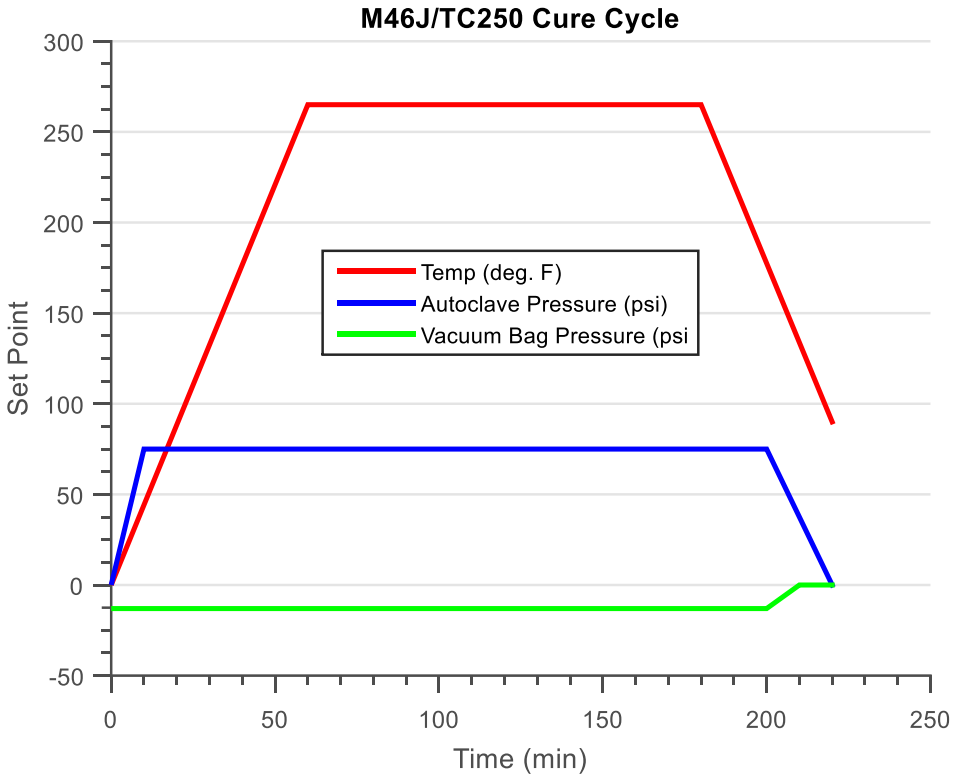

Figure 32 Cure cycle of M46J/TC250 pre-preg [44].

Appendix B. Parametric Study Results

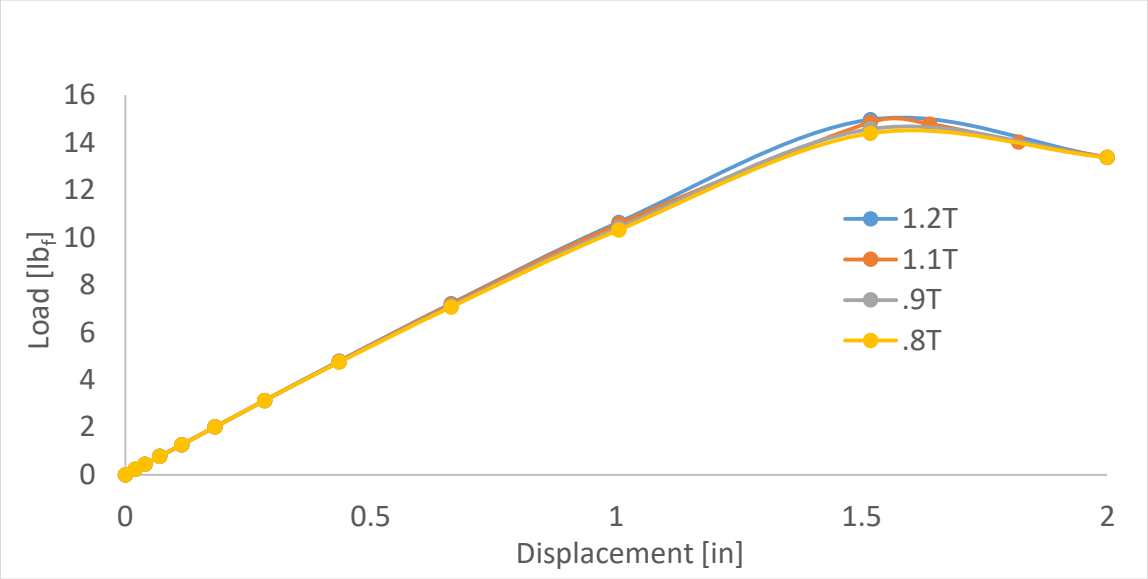

Figure 33 DCB P-δ curve for 80%-120% range of initially converged normal traction of cohesive contact interaction.

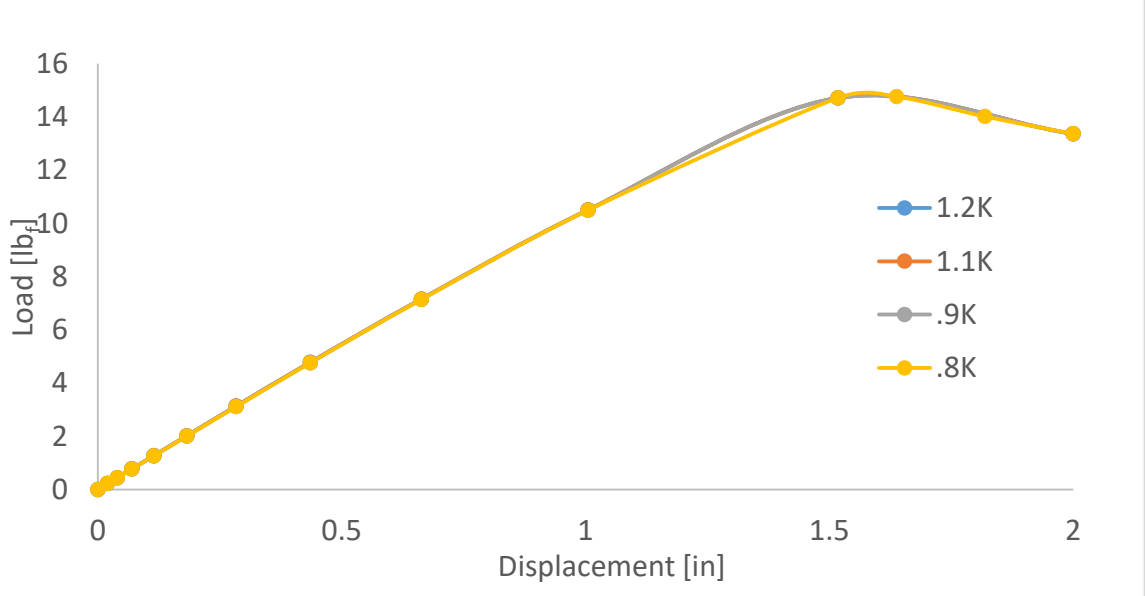

Figure 34 DCB P-δ curve for 80%-120% range of initially converged cohesive stiffness of cohesive contact interaction.

Appendix C. Abaqus/Standard Input File

```
*Heading
** Job name: k-10 Model name: Josh_Model_M46J_6-2-16
** Generated by: Abaqus/CAE 6.14-2
*Preprint, echo=NO, model=NO, history=NO, contact=NO
**
** PARTS
**
*Part, name=bot
*End Part
**
*Part, name=top
*End Part
**
**
** ASSEMBLY
**
*Assembly, name=Assembly
**
*Instance, name=bot-1, part=bot


*Orientation, name=Ori-1
1., 0., 0., 0., 1., 0.
3, 0.
** Section: Section-1
*Solid Section, elset=Set-1, orientation=Ori-1, material=Comp-M46J
```

```
*Element, type=CPE4R


*Orientation, name=Ori-1
1., 0., 0., 0., 1., 0.
3, 0.
** Section: Section-1
*Solid Section, elset=Set-1, orientation=Ori-1, material=Comp-M46J


**
** MATERIALS
**
*Material, name=Comp-M46J
*Elastic, type=ENGINEERING CONSTANTS
 3e+07, 1.2e+06, 1.2e+06,     0.3,     0.3,     0.4, 1.2e+06, 1.2e+06
   1e+06,
**
** INTERACTION PROPERTIES
**
*Surface Interaction, name=IntProp-1
1.,
*Cohesive Behavior, eligibility=SPECIFIED CONTACTS
 1e+07, 1e+07, 1e+07
*Damage Initiation, criterion=QUADS
1000.,1000.,1000.
*Damage Evolution, type=ENERGY
 1.5,
**
** INTERACTIONS
```

```
**
** Interaction: Int-1
*Contact Pair, interaction=IntProp-1, small sliding, type=SURFACE TO SURFACE, adjust=0.0
s_Surf-9, m_Surf-9
*Initial Conditions, type=CONTACT
s_Surf-9, m_Surf-9,
** ----------------------------------------------------------------
**
** STEP: Step-1
**
*Step, name=Step-1, nlgeom=YES, extrapolation=NO, inc=10000
*Static
0.001, 0.005, 1e-07, 1.
**
** BOUNDARY CONDITIONS
**
** Name: bot Type: Displacement/Rotation
*Boundary
Nbot, 1, 1
Nbot, 2, 2, -0.1
** Name: top Type: Displacement/Rotation
*Boundary
Ntop, 1, 1
Ntop, 2, 2, 0.1
**
** CONTROLS
**
*Controls, reset
*Controls, analysis=discontinuous
```

```
*Controls, parameters=time incrementation
, , , , , , , 30, , ,
**
** OUTPUT REQUESTS
**
*Restart, write, frequency=0
**
** FIELD OUTPUT: F-Output-1
**
*Output, field
*Node Output
CF, RF, RT, U
*Element Output, directions=YES
LE, PE, PEEQ, PEMAG, S
*Contact Output
CDISP, CSTRESS
**
** HISTORY OUTPUT: H-Output-1
**
*Output, history
*Node Output, nset=Ntop
RF2, U2
*End Step
```

Appendix D. Summary of Testing Procedures

ASTM D5528

- Connect hinge fixtures to bonded hinges of DCB specimen via steel pins.
- Load DCB specimen into Instron® grips.
    - Insert top-sub-laminate hinges into upper-jaw
    - Raise lower-jaw and insert bottom sub-laminate hinge into lower-jaw
- Mount USB microscope such that the delamination front is observed with an accuracy of ± 0.5mm.
- Load specimen at constant displacement rate of 0.001in/sec.
    - Record load and displacement on data acquisition software.
    - Pause loading after approximately 3-5mm of delamination growth.
    - While paused, mark position of the tip of the pre-crack. This will be used for subsequent pre-cracked test.
    - Change displacement rate to -0.001in/sec. and unload specimen. Do not overload specimen in a compressive state. The negative displacement rate corresponds to closing the opened displacement achieved during initial loading.
- Change displacement rate back to 0.001in/sec. and reload specimen until crack has extended at least 50mm (~2in) past pre-crack location
    - Record load and displacement
    - Unload specimen and properly remove from Instron®.

ASTM D7905

- Set span of ENF fixture to 4in.
- Place ENF test specimen into fixture such that 20mm of crack length is within the span of the ENF fixture.
- Insert the loading fixture into upper-jaw of Instron®
- Rest ENF fixture on lower-jaw. Lower the upper-jaw such that the loading fixture is slightly above the top of the ENF fixture. Do not lower too much and load the specimen.
- Load ENF specimen to approximately 100-125lbs with displacement rate of -0.001in/sec. (compressive state). Record load and displacement.
    - Pause load.
    - Change displacement rate to 0.001in/sec and lower bottom-jaw until the ENF specimen is not loaded.
- Make sure enough space is between loading fixture and ENF fixture for safe removal of ENF fixture from vicinity of the Instron® jaws.
- Remove ENF fixture
- Re-position test specimen such that 40mm of crack length is within the span of the ENF fixture.

- Insert the loading fixture into upper-jaw of Instron®
- Rest ENF fixture on lower-jaw. Lower the upper-jaw such that the loading fixture is slightly above the top of the ENF fixture. Do not lower too much and load the specimen.
- Load ENF specimen to approximately 100-125lbs with displacement rate of -0.001in/sec. (compressive state). Record load and displacement.
    - Pause load.
    - Change displacement rate to 0.001in/sec and lower bottom-jaw until the ENF specimen is not loaded.
- Make sure enough space is between loading fixture and ENF fixture for safe removal of ENF fixture from vicinity of the Instron® jaws.
- Remove ENF fixture
- Re-position test specimen such that 30mm of crack length is within the span of the ENF fixture.

- Insert the loading fixture into upper-jaw of Instron®
- Rest ENF fixture on lower-jaw. Lower the upper-jaw such that the loading fixture is slightly above the top of the ENF fixture. Do not lower too much and load the specimen.
- Load ENF specimen until critical load is achieved. Record load and displacement.
- Pause loading and change displacement rate to 0.001 to lower bottom-jaw.
- Remove ENF fixture from Instron®.

4ENF

- Set upper span to 2.5 in
- Set lower span to 4.5 in
- Place 4ENF test specimen into 4ENF fixture. Position specimen such that desired delamination length is within the lower span of the 4ENF fixture.
- Insert loading fixture into upper-jaw of Instron®.
- Take 4ENF fixture and rest on the lower-jaw of the Instron®.
- Lower the upper-jaw such that the loading fixture is slightly above the top of the 4ENF fixture.
- Load specimen at displacement rate of -0.001in/sec. (compressive state). Record load and displacement.
    - If observing crack propagation is desired, continue loading of specimen after critical load is achieved.
    - Operator discretion advised: if the complete failure of test specimen is not desired, make sure to pause load and unload specimen after 3-5mm of crack growth has occurred such that the specimen will be intact.
- Pause and unload specimen.
- Remove from Instron®.